Renewable Syngas Generation and Biogas/Landfill Gas Upgrade via Thermocatalytic Conversion of Carbon Dioxide

by

Yichen Zhuang

A thesis
presented to the University of Waterloo
in fulfillment of the
thesis requirement for the degree of
Master of Applied Science
in
Chemical Engineering

Waterloo, Ontario, Canada, 2017

AUTHOR'S DECLARATION

I hereby declare that I am the sole author of this thesis. This is a true copy of the thesis, including any required final revisions, as accepted by my examiners.

I understand that my thesis may be made electronically available to the public.

Abstract

The reverse water gas shift (RWGS) and thermocatalytic Sabatier reaction can be potentially used to convert captured CO_2 or biogas/landfill gas into renewable synthetic fuels via syngas generation or production of renewable natural gas. However, these conversion pathways have not been yet realized because of a number of technological challenges, including a lack of catalysts that possess satisfactory catalytic performance. Also, biogas and landfill gas are rich in both carbon dioxide (CO_2) and methane (CH_4) so the CO_2 content (up to 50vol%) has to be eliminated prior to the use.

In the first part of this research project, the RWGS reaction over the 0.5wt% Ru-promoted 40wt% $Cu/ZnO/Al_2O_3$ catalyst is studied. Due to the Ru addition, CO_2 conversion was improved by over 100% as compared to the baseline $Cu/ZnO/Al_2O_3$ catalyst. The catalyst stability was significantly improved as well. Although Ru is known for its high activity in methanation reactions, the 0.5wt% $Ru-Cu/ZnO/Al_2O_3$ catalyst maintained complete selectivity to CO formation. In order to investigate this intriguing finding, a series of catalysts were synthesized by gradually removing the catalyst components and varying the synthesis procedure. It has been found that the Ru-support interaction and Ru oxidation state are crucial factors with respect to CH_4 formation suppression.

As an alternative to CO_2 separation, CO_2 contained in biogas and landfill gas can be potentially converted into synthetic CH_4, upgrading these waste streams to a pipeline quality renewable natural gas (RNG). In the second part of this research project, a series of 0.02-1wt% $Ru/\gamma-Al_2O_3$ catalysts were evaluated for their performance in a single-pass conversion of 50:50 CO_2/CH_4 mixture into synthetic CH_4. For the 0.1-0.5wt% Ru catalysts, CO_2 conversion of as high as 80% was achieved at 450 °C, while maintaining 95% selectivity to CH_4 production over CO. These catalysts also showed excellent stability that, alongside with superior selectivity and good conversion, opens a possible avenue for practical applications.

Key words: RWGS reaction, Sabatier reaction, $Cu/ZnO/Al_2O_3$, Ru/Al_2O_3, landfill gas, biogas upgrade.

Acknowledgements

I would first like to thank my supervisor Professor David Simakov for his patience, continuous support and guidance throughout my Master's program.

I would also like to thank my committee members: Professor Hector Budman, Professor Michael Pope for their precious comments and suggestions on my research project.

This work would not have been possible without the help and advice from Yun Bai, Robert Currie, Faisal Khan, Sogol Tabar, Guanjie Sun and Alex McGowan.

Last but not least, I would like to express my gratitude to my parents and friends for their support and encouragement.

This project was funded by the Natural Science and Engineering Research Council (NSERC) of Canada through the NSERC Discovery Grant Program.

Table of Contents

List of Figures

List of Tables

Chapter 1
Introduction

1.1 Problem Statement

Global warming is having a more and more significant effect on the climate and everyday life. As Figure 1 shows, carbon dioxide (CO_2) and methane (CH_4) contribute the majority of the total greenhouse gases (GHGs) emission for the past five decades. Since the industrial revolution, the extensive use of fossil fuels caused accelerating rates of CO_2 pollution. As atmospheric CO_2 levels have continued to climb in recent years, the need to significantly reduce anthropogenic CO_2 emissions has become more urgent [2]. On the other hand, CH_4 is another greenhouse gas that is 25 times stronger that CO_2 in terms of the global warming potential [3]. Waste streams such as biogas and landfill gas contain 50-70% CH_4 and 25-45% CO_2, both being GHGs [4-5]. On the other hand, biogas and landfill gas are also potential renewable streams as they are produced via anaerobic fermentation process, thus not of fossil origin. In 2015, around 56 billion cubic meters of biogas was produced globally [6].

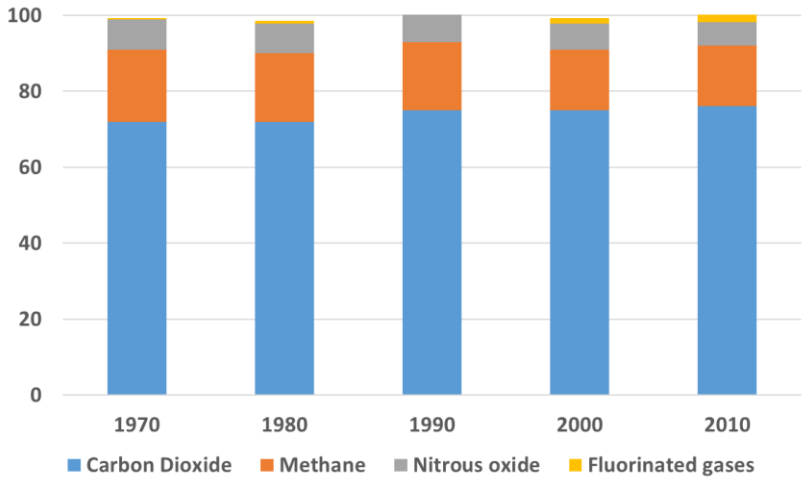

Figure 1. Global greenhouse gas emission by gas [1].

Since most countries are controlling GHGs emissions, technologies to capture and sequestration CO_2 are being developed. Captured CO_2 from fossil fuel powered power plants is transported, stored and used for other purposes such as enhanced oil recovery. CH_4 from biogas and landfill is usually used as fuel after purification and CO_2 separation. The problem with the current technologies is that they are not cost effective and their processing capacity is not adequate to accommodate accelerating emissions of GHGs.

Alternatively, CO_2 sequestration could be followed by CO_2 conversion into synthetic fuels and chemicals. Converting CO_2 into useful chemicals is of particular interest as this approach allows for CO_2 recycling and introducing of renewable energy into the chemical industry production chain [7-9]. There are several optional pathways to synthesize fuels and chemicals using CO_2 as a carbon source, including photo and electro-chemical reduction, biological conversion, and thermocatalytic hydrogenation [10]. The implementation of the photo and electro-chemical CO_2 reduction routes has a significant potential but is limited by the low CO_2 solubility in water and transport limitations [10-12]. The cost of cultivating and maintaining biomass growth systems remains a prohibiting factor for the implementation of the large-scale biofuel production [10].

As an alternative to the abovementioned options, the thermocatalytic conversion of CO_2 can be seen as a viable option due to its technical feasibility, considering its similarity to some well-established industrial processes [10]. Options include reverse water gas shift reaction (RWGS) Eq. (1) and methanation reaction Eq. (2-3) [13]. By thermocatalytic conversion, CO_2 can be converted into synthetic natural gas (SNG) or syngas.

$$CO_2 + H_2 \rightleftarrows CO + H_2O \qquad \Delta H^{\circ}_{298} = 41 \text{ kJ/mol} \tag{1}$$

$$CO_2 + 4H_2 \rightleftarrows CH_4 + 2H_2O \qquad \Delta H^{\circ}_{298} = -164.9 \text{ kJ/mol} \tag{2}$$

$$CO + 3H_2 \rightleftarrows CH_4 + H_2O \qquad \Delta H^{\circ}_{298} = -206.1\ \text{kJ/mol} \qquad (3)$$

If CO_2 is reduced to CO via the RWGS reaction the produced syngas can be later utilized to produce methanol and hydrocarbons via the Fischer-Tropsch process [14, 15]. This option provides the flexibility in types of product and the high efficiency for conversion of CO_2 captured from various waste streams, i.e., flue gases [14]. If methanation pathway is used, CO_2 can be reduced to CH_4 and used as Renewable Natural Gas (RNG). For thermocatalytic conversion of biogas and landfill gas, the use of pure CO_2 as a feedstock might be less economical due to high capital and operational cost associated with separating high concentration of CH_4 in the feed prior to the reaction. In this case, an approach that does not require CO_2 separation from biogas/landfill gas is apparently more attractive. Direct biogas/landfill gas upgrade into Renewable Natural Gas via CO_2 methanation is apparently a better choice in this case, to increase the overall CH_4 production as well as avoid CO_2 separation cost.

1.2 Project Objective

The objective of this project is to identify suitable catalysts for both syngas production and biogas/landfill gas upgrade via thermocatalytic CO_2 hydrogenation (these pathways are shown in Figure 2, among other thermocatalytic pathways). Catalyst to be identified need to have high CO_2 conversion, high selectivity to desired product and good resistance to deactivation. Based on the critical analysis of the literature, Ru-Cu/ZnO/Al_2O_3 and Ru/Al_2O_3 catalyst were suggested as potential formulations for the RWGS and Sabatier reactions, respectively.

The specific goals related to the project objective are listed as follows:

1. Evaluate the catalyst performance in terms of CO_2 conversion, CO or CH_4 generation selectivity, and stability over the range of temperatures, space velocities, and other relevant operating conditions.
2. Investigate the results of the catalytic performance evaluation to understand the mechanisms of the catalytic activity and selectivity to certain products, as well as the mechanism of the catalyst deactivation.

1.3 Thesis Outline

This thesis consists of two studies on the Ru-promoted $Cu/ZnO/Al_2O_3$ and Ru/Al_2O_3 catalysts. Thesis chapters are summarized as follows:

Chapter 2 gives the background for the CO_2 thermocatalytic conversion, including possible reaction pathways, individual reactions, as well as current technical limitations. Chapter 2 also reviews past and recent literature on RWGS and methanation catalysts. Chapter 3 presents the methodology for the catalytic performance evaluation, including catalyst preparation, experimental flow system setup, experiment design, and data processing.

Chapter 4, 5, and 6 include the experimental results of the catalytic performance evaluation, catalyst characterization results, and conclusion drawn from the analyzed data. The results of the catalytic performance evaluation over various reaction conditions and stability tests are shown and discussed in Chapter 4. Chapter 5 focuses on the catalyst characterization conducted by ICP-MS, SEM-EDS, TEM, XRD, TGA-MS and some other catalyst characterization techniques. These results were analyzed leading to the discussion on reaction mechanisms, including activity, selectivity, and stability. Chapter 6 concludes the results obtained and discusses future direction related to the project.

Chapter 2
Background and Literature Review

2.1 Background of thermocatalytic conversion of CO_2

2.1.1 Reaction pathways

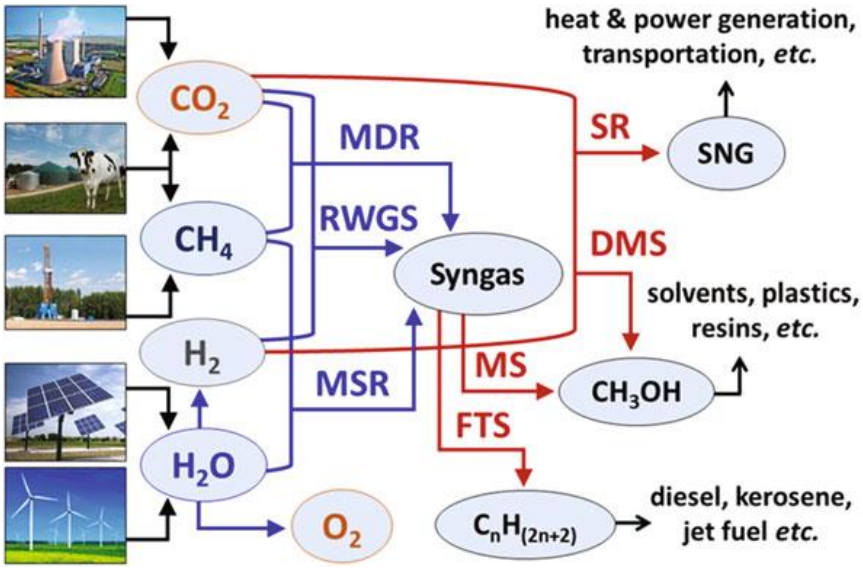

Figure 2. Reaction pathways of producing synthetic fuels and chemicals from CO_2 [10].

The reaction pathways of producing synthetic fuels and chemicals from carbon dioxide is shown in Figure 2. The source of hydrogen can be versatile and cheaper sources can help reduce the overall production cost from CO_2 hydrogenation. Gasification of biomass and coal, or water electrolysis with off-peak, surplus electricity and renewable energy are suitable hydrogen source. From thermocatalytic conversion of CO_2 with hydrogenation, syngas can be obtained via either RWGS reaction or methane dry reforming (MDR). Syngas can also be produced with CH_4 and water via methane steam reforming (MSR). Syngas is a useful chemical feedstock which can be further converted into chemicals and fuels like methanol and higher hydrocarbons via Fischer-Tropsch process. Another important pathway of CO_2 and H_2 is generating synthetic natural gas

(SNR) via methanation reaction. The ultimate goal is building large-scale industrial plants producing chemicals using thermocatalytic conversion of captured CO_2, which can recycle carbon dioxide and reduce the consumption of fossil fuels. Among all the components in this process the catalytic reactor is the core technology. Currently there is neither well-developed reactor design nor suitable catalyst with satisfying performance available for this process.

2.1.2 Reverse water gas shift

Water gas shift reaction was originally developed to provide affordable hydrogen for ammonia synthesis. Reverse water gas shift, on the other hand, produce carbon monoxide (CO) and water (H_2O). It was estimated that producing liquid fuel via RWGS reaction is more energy efficient than other routes (biomass gasification with H_2, algae oil, photosynthetic conversion) [16]. Also, as compared to alternative technologies the RWGS reaction is more feasible as it can rely on currently existing technology for thermocatalytic conversions. The RWGS reaction is endothermic, so high CO_2 conversion will be achieved at relatively high temperature due to the equilibrium limitation. However, at high temperature coking and CH_4 formation tend to happen, which could cause either catalyst deactivation or low CO selectivity. At 1000 K, increasing H_2:CO_2 ratio from 1 to 1.8 can result in 30% improvement of CO_2 equilibrium conversion, while separating excess H_2 can also potentially cause high operational cost [17]. A study showed that at high temperature and pressure, the activation energy of RWGS reaction reduced from 75 to 51 kcal/mol and this phenomenon is still under investigation [18].

2.1.3 Sabatier Reaction (CO_2 Methanation)

CO_2 methanation reaction, as known as Sabatier reaction, is a highly exothermic reaction. CO_2 methanation is usually accompanied by RWGS Eq. (1) and CO methanation Eq. (3). For 1 m^3/h CH_4 production rate (STP), 1.8 and 2.3 kW heat can be released from CO_2 and CO methanation

respectively [19]. As shown in Figure 3, the thermodynamic equilibrium of CO_2 methanation favors high pressure and low temperature, while it is hard for these exothermic reactions to reach equilibrium conversions at low temperature [20]. Running at high temperature could cause sintering of the catalyst, which further leads to the loss of structural strength and catalyst deactivation [21]. High CO concentration can cause formation of carbonyl and gum, which will also result in catalyst deactivation [21].

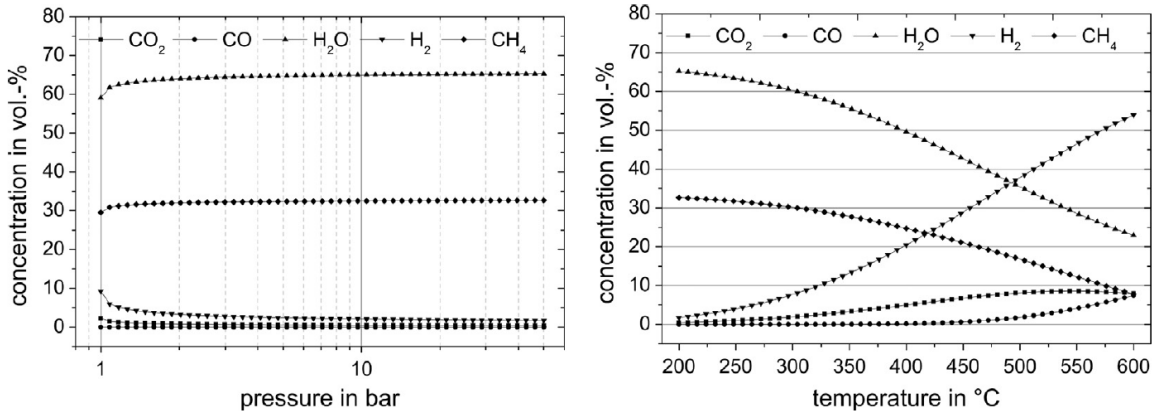

Figure 3. Equilibrium concentration of CO_2 methanation as a function of pressure (at temperature=300 °C) and temperature (at pressure =1 bar). Feed composition H_2:CO_2=4 [19].

To maintain the reactor temperature at relatively low temperature, proper cooling is required for the Sabatier reactor. A new reactor design for Sabatier reaction was proposed and the schematic is shown in Figure 4. Model results indicated that the heat removal was efficient thus CH_4 production could be maximized and catalyst deactivation could be further suppressed [22].

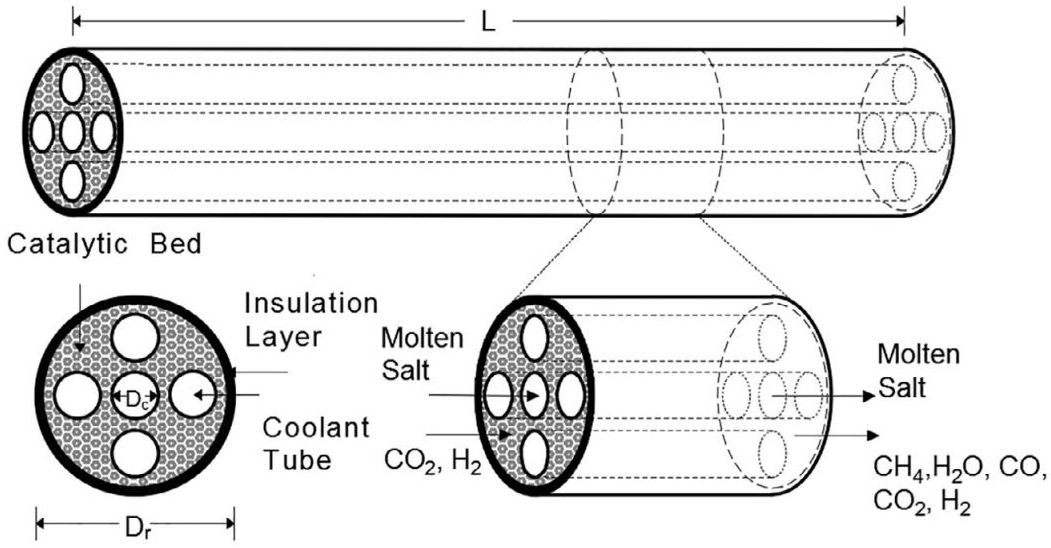

Figure 4. Sabatier reactor design with molten salt cooling [22].

2.2 Biogas and landfill gas processing and utilization

Current landfill gas is mostly used as fuel (direct use) in boiler system for heating purposes or gas engine to generate electricity. For these applications the quality of gas does not have to be high, so the processing of landfill gas prior combustion is simple, which only removes particles in stream [23]. For uses that require high heat value, a secondary treatment removes CO_2, contaminants and other volatile organic compounds [24]. The potential use of landfill gas includes upgrading to conventional natural gas, fuel for vehicles and fuel cells and evaporation of the leachate in landfill.

The utilization of biogas is similar to landfill gas shown in Figure 5. Biogas is burnt to power boiler and generator or upgraded into natural gas. Biogas cleaning and upgrading technologies involves water scrubbing (removal of H_2S and CO_2), cryogenic separation (CO_2 removal), physical absorption (CO_2 removal), chemical absorption (CO_2 removal), pressure swing adsorption (N_2, O_2 and CO_2 removal), membrane separation (H_2S and CO_2 removal) and in-situ enrichment [26].

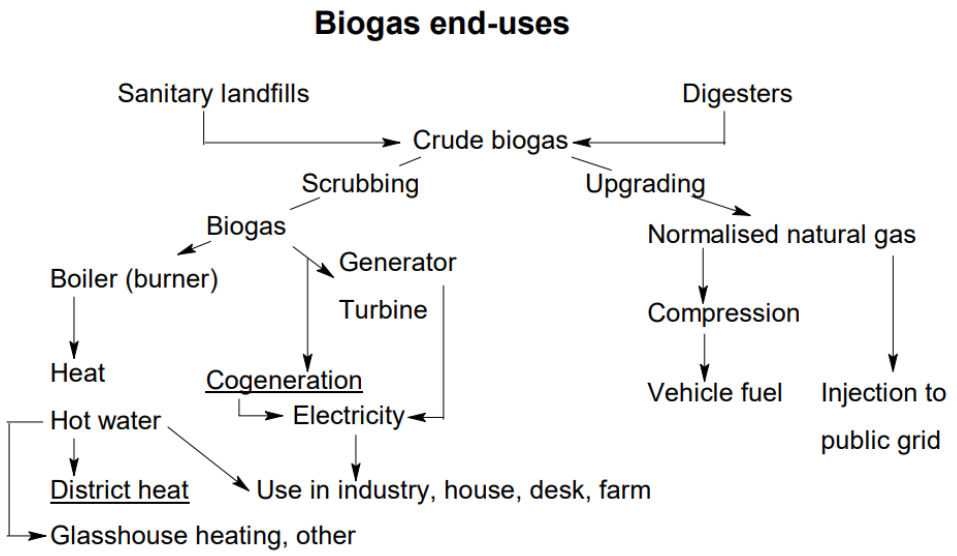

Figure 5. Biogas utilization [25].

2.3 Reverse water gas shift catalysts

2.3.1 Noble metal catalysts

Supported Pt, Rh and Pd catalysts have been found to be active to RWGS reaction. Chen et al. found that 1wt% Pt/TiO_2 catalyst could achieve 20% CO_2 conversion at 400°C with H_2:CO_2=1 and total gas flow at 50mL/min [27]. The active site of CO formation was found to be Pt-O_v-Ti^{3+} formed at the interface of Pt and TiO_2 instead of large Pt particles, and the latter one tended to form CH_4 at high temperature [27]. Goguet et. al. suggested high CO concentration caused increasing carbon deposition on catalyst surface and deactivation by conducting TPO experiments on 2% Pt/CeO_2 catalyst [28]. CO_2 conversion over Pd-based membrane was found to achieve 10% at 723 K and H_2:CO_2=3, and operating pressure was found to have a strong impact on CO_2 conversion [29].

2.3.2 Cu-based catalysts

Currently some water gas shift catalysts are also used in reverse water gas shift due to the reversibility of the reaction. For example, Cu-based catalysts, which are one of commercial WGS catalysts, also showed some activity in RWGS. One of the most commonly used catalyst for reverse water gas shift reaction is $Cu/ZnO/Al_2O_3$. As such, this catalyst has been extensively studied. It is well known that at low temperatures, Cu/ZnO catalysts can catalyze both the forward and reverse water-gas shift reactions, with little to no methane (CH_4) formed as a side product.

The RWGS also plays an important role in the synthesis of methanol from CO_2 and Cu/ZnO-based formulations have been considered as promising catalysts for methanol synthesis by direct CO_2 hydrogenation [30]. While commercial Cu-based catalysts show good conversion and selectivity in methanol synthesis, they are often prone to deactivation by sintering and coking [31]. Common coking mechanisms in the RWGS reaction are the Boudouard reaction, Eq. (4), and CO reduction (reverse gasification), Eq. (5), [32]:

$$2CO \rightleftarrows C + CO_2 \qquad \Delta H^o_{298} = -173.3 \text{ kJ/mol} \tag{4}$$

$$CO + H_2 \rightleftarrows C + H_2O \qquad \Delta H^o_{298} = -131.3 \text{ kJ/mol} \tag{5}$$

In order to extend the lifetime of Cu/ZnO-based catalysts, a substantial amount of work on studying the effects of adding various metal oxides has been conducted. Al_2O_3, Ga_2O_3, ZrO_2 and Cr_2O_3 have all been found to increase the activity of Cu/ZnO catalysts. Al_2O_3 and ZrO_2 increased the catalytic activity by improving copper particle dispersion, while Ga_2O_3 and Cr_2O_3 have been found to increase the specific activity per unit of Cu surface area [33]. Improving the stability of Cu/ZnO catalysts has been also achieved by adsorbing small amounts of colloidal silica on the precipitate; the activity of the $Cu/ZnO/ZrO_2/Al_2O_3$ catalyst containing 0.6 wt% silica in methanol synthesis was maintained for 500 h [33].

For the RWGS reaction, $Cu/ZnO/Al_2O_3$ catalysts with Cu:(Cu+Zn) ratios of 0.25 and 0.75 have been found to achieve 5% and 15% CO_2 conversion respectively using H_2:CO_2 = 1 at 515 K and 1 bar [34] . Meanwhile, the Cu/ZnO catalyst without the alumina support achieved up to 12% CO_2 conversion under the same conditions with a Cu:(Cu+Zn) ratio of 0.7. These findings indicated the significant effect of the Cu/Zn ratio on the catalyst performance [34]. Effect of the feed composition was also studied suggesting that the H_2/CO_2 ratio higher than 3 is essential for the RWGS reaction [35]. It was suggested that a phase transition of the $Cu/ZnO/Al_2O_3$ catalyst occurs at high H_2/CO_2 ratios improving the catalyst activity [35]. As for the reaction mechanism, formate species were suggested as an important intermediate for CO formation in the RWGS reaction [36].

Although a substantial number of materials have been studied for the RWGS reaction, including transition and noble metals, and transition metal carbides [14], RWGS catalysts that possess high catalytic activity while maintaining good stability are still to be identified. The $Cu/ZnO/Al_2O_3$ catalyst is an attractive option due to its low cost and virtually complete selectivity to CO production. However, the $Cu/ZnO/Al_2O_3$ catalyst activity is relatively low and the stability of this catalyst at elevated temperatures, which are required to achieve high RWGS conversion, is poor.

2.4 Methanation catalysts

2.4.1 Ni-based catalysts

Most commonly used commercial methanation catalyst is Ni-based catalyst. Though Ni is not the most active metal for methanation, its performance per unit cost is excellent [37]. The support of nickel catalyst is usually alumina, sometimes acid-washed kieselguhr [38]. CO_2 conversion and CH_4 selectivity of 20 wt% Ni/Al_2O_3 catalyst are around 81% and 96% respectively under 400°C and 55,000 h^{-1} [39]. It has been found that addition Yb_2O_3 can significantly improve the stability

and dispersion of Ni/Al_2O_3 catalyst (long-term stability is one of the major concerns in the use of Ni-based catalysts) [40]. Using Y_2O_3 as a sole support was also demonstrated, obtaining 76% CO_2 conversion and 100% CH_4 selectivity at 300 °C and H_2:CO_2 = 4 over the Ni/Y_2O_3 catalyst [41]. Other supports such as SiO_2 and MgO were also studied showing generally good performance over short operation periods [42-43]. For Ni-based catalyst, CO was confirmed as an intermediate, indicating the reaction pathway via CO [41]. One of the drawbacks with the use of Ni-based catalysts is CO formation which can be significant, as CO was confirmed as a reaction intermediate for Ni-catalyzed methanation [41]. Addition of MgO to Ni/Al_2O_3 catalyst can prevents the rapid carbon formation but it still requires a better coking resistance [44].

2.4.2 Transitional metal carbides

Transitional metal carbides (TMCs) are interesting materials, since they have electronic structures similar to those of precious metals, providing high catalytic activity [45]. Among those TMCs molybdenum, cobalt, nickel and iron carbide are mostly studies for CO and CO_2 hydrogenation [46-49]. CO_2 conversion over β-Mo_2C was around 24% at 300°C under 2MPa, while bimetallic carbide Co/M_2C had a CO_2 conversion at 31% under the same condition [47]. Modified $K/Ni\text{-}Mo_2C$ and $K/Co\text{-}Mo_2C$ were found to have a CO_2 conversion at 59.2% and 51.1% respectively under 2MPa and 613 K [46]. TMCs are relatively new material and not well studied, they might have a huge potential in the future.

2.4.3 Supported noble metal catalysts

The activity of noble metal has been studied and listed from high to low: Ru, Ir, Rh, Os, Pt, Pd [50]. CO_2 conversion of 55% and CH_4 selectivity of 95% were demonstrated over the 5 wt% Ru/Al_2O_3 catalyst at 350 °C and H_2:CO_2 = 3 [51]. After testing Ru/Al_2O_3 catalysts with Ru loading ranges from 0.1-5 wt%, it was found that high metal dispersion could cause high selectivity to CO

[51]. It is also concluded that size of Ru nanoparticles is relevant to catalytic activity of hydrogenation [52]. Combination of Ru and Ni, bimetallic Ni–Ru/γ-Al_2O_3 was found to have even better performance [53]. Other than Ru, Pd and Pt also showed certain activity towards methanation, while their performance strongly depends on the support [54-55].

Chapter 3
Experimental Setup

3.1 Catalyst preparation

3.1.1 Cu/ZnO/Al_2O_3 RWGS catalyst

The baseline Cu/ZnO/Al_2O_3 catalyst (denoted as Cu/ZnO) was synthesized using a co-precipitation method. The ratio of Cu, ZnO and Al_2O_3 was kept at 40:50:10 wt%. Required amounts of 1 M solutions of copper nitrate ($Cu(NO_3)_2 \cdot 6H_2O$, Sigma Aldrich), zinc nitrate ($Zn(NO_3)_2 \cdot 3H_2O$, Sigma Aldrich), and aluminum nitrate ($Al(NO_3)_3 \cdot 9H_2O$, Sigma Aldrich) were dropwise added to a 1 M solution of sodium bicarbonate ($NaHCO_3$, Alfa Aesar) under vigorous stirring at 60 °C. After 24 hours of aging, the resulted precipitate was filtered, washed and dried overnight under air at 110 °C. The dried precipitate was calcined under a continuous flow of air at 350 °C for 4 h, pelletized (40 MPa), crushed, and sieved to 250-425 μm particles. Before the reaction, the catalyst was reduced under H_2 flow at 250 °C for 1 hour.

3.1.2 Ru promoted RWGS catalyst

The 0.5wt% Ru-Cu/ZnO/Al_2O_3 catalyst (denoted as Ru-Cu/ZnO) was prepared by wet impregnation using ruthenium chloride ($RuCl_3 \times H_2O$, Alfa Aesar) as a source of Ru and the uncalcined precipitate prepared as described above (after overnight drying at 110 °C). For comparison, one sample was prepared using the calcined precipitate (after calcination under air flow at 350 °C for 4 h). For wet impregnation, the precipitate (either calcined or uncalcined) was added to an appropriate amount of ruthenium chloride dissolved in acetone. The resulted slurry was sonicated for 30 min in a 20 mL vial placed in an ultrasonic bath (Fisher Scientific, CPX962118R), dried at 60 °C in air, pelletized (40 MPa), crushed, and sieved to 250-425 μm

particles. The Ru-ZnO/Al_2O_3 and Ru/Al_2O_3 catalysts (denoted as Ru-ZnO and Ru, respectively) were prepared by the same method as described above (using the uncalcined precipitate), but removing the Cu or Zn precursors, while keeping the Ru content at 0.5wt% Ru. The ZnO:Al_2O_3 weight ratio in the ZnO/Al_2O_3 support was kept at 5:1.

3.1.3 Ru/Al_2O_3 methanation catalyst

A series of Ru/γ-Al_2O_3 catalysts with Ru loading ranging 0.02-1wt% were prepared using a wet impregnation method [56]. Commercial alumina support pellets (γ-Al_2O_3, 250 m^2/g, Alfa Aesar) were crushed and sieved to 250-425 μm particles prior to impregnation. Appropriate amounts of ruthenium chloride ($RuCl_3 \times H_2O$, 37.5wt% Ru, Alfa Aesar) were dissolved in acetone (99.5%, Fisher Scientific) and the sieved γ-Al_2O_3 particles were added to the solutions with different Ru concentrations. The resulted slurries were sonicated for 30 min in 20 mL vials placed in an ultrasonic bath (Fisher Scientific, CPX962118R). After sonication, the slurries were dried in air at 60 °C.

3.2 Flow system setup

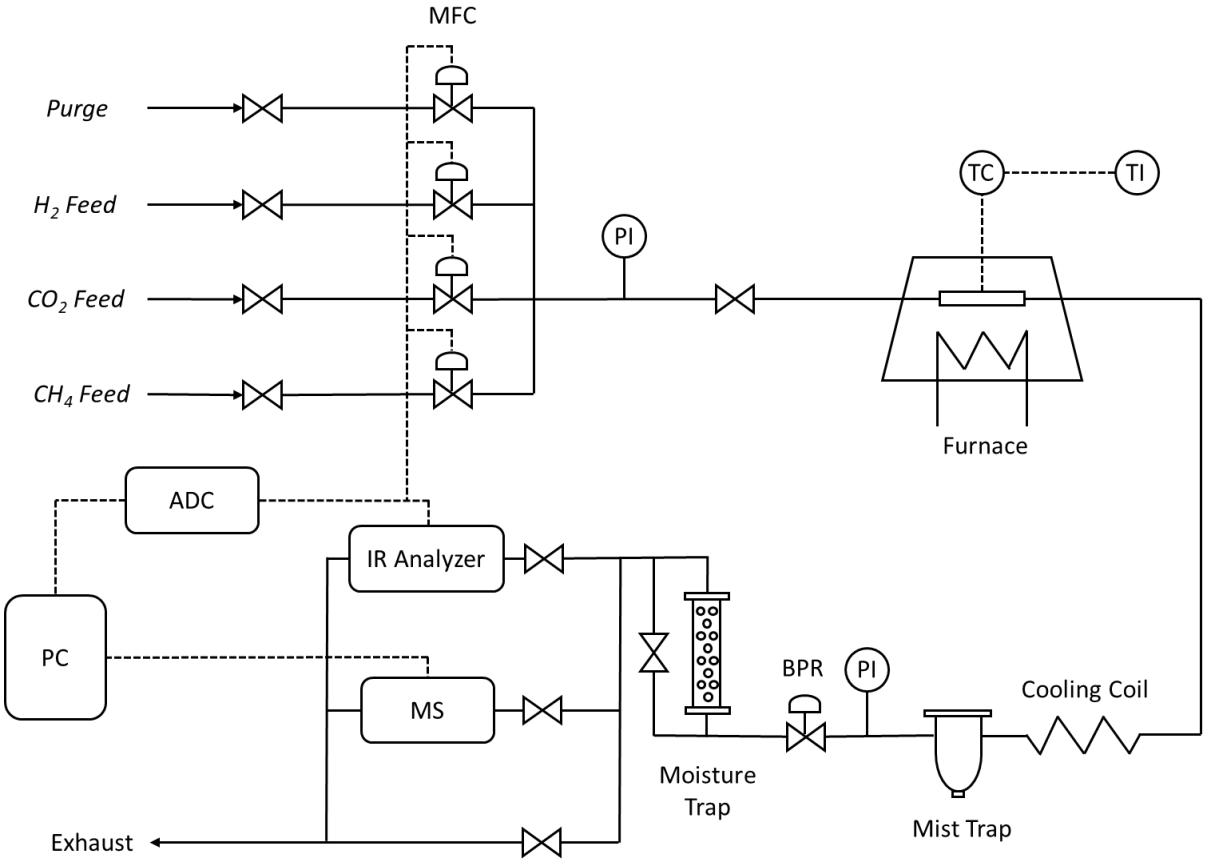

Figure 6. Flow system setup for catalytic performance evaluation.

The experimental setup for catalytic performance evaluation is shown in Figure 6. Two mass flow controllers were used to control CO_2 and H_2 feed to the reactor. The reactor was made from a 1/4″ stainless steel union tee (Swagelok) connected to a 1/4″ stainless steel tubing on both sides (Swagelok), with a type K type thermocouple (1/8″, Omega Engineering, Inc.) placed in a direct contact with the catalytic bed. The catalyst was loaded through the remaining tee opening, which was consequently sealed with a plug (Swagelok). The reactor was placed in a furnace (Thermo Fisher Scientific, Lindberg/Blue M™ Mini-Mite™ Tube Furnaces) with the tee containing the catalyst being in the middle of the furnace. The temperature was controlled with a furnace built-in

temperature controller (UP150, Yokogawa) using the thermocouple installed within the reactor (in contact with the catalytic bed). A back-pressure regulator (Swagelok, S01094789B) was used to adjust the reactor pressure. Water was removed from the outlet stream using a mist trap (SMC Corporation, AFM40-N02-Z-A) installed before the back-pressure regulator, Figure 6, and a silica gel column (Agilent Technologies, 5182-9411, the original adsorbent was replaced with orange silica gel, Fisher Scientific). Concentrations of CO, CO_2 and CH_4 in the outlet stream were measured on a dry basis (after the removal of water and moisture) with the IR analyzer (IR-208, Infrared Industries, Inc., USA) continuously monitored using an analog-to-digital converter (USB 6008, National Instruments) and LabVIEW (National Instruments).

3.3 Catalyst characterization

Chemical composition was verified using inductively coupled plasma mass spectrometry (ICP-MS, Prodigy SPEC, Leeman Labs Inc.). Specific surface area (SSA) was measured by a surface area analyzer (Gemini VII 2390, Micromeritics Instrument Corporation) using nitrogen as adsorption gas. Thermal gravimetric analysis (TGA) of spent catalysts was conducted to determine the extent of coking (Q500, TA Instruments). Temperature ramp was set to 10 °C/min for $T \leq 150$ °C and 2 °C/min for T = 150-800 °C (for Ru/Al_2O_3 catalyst maximum temperature was 600 °C) and the air flow of 40 ml/min. The corresponding temperature programmed oxidation (TPO) was conducted under identical conditions using a mass spectrometer (MS) (HPR-20, Hiden Analytical) and an FTIR analyzer (MultiGas™ 2030, MKS Instruments) to measure O_2, CO, and CO_2 in the reactor outlet. X-ray diffraction (XRD) patterns were obtained using a D8 Discover diffractometer (Bruker). Transition electron microscope (TEM) micrographs were obtained using a Zeiss microscope (100 kV). Elemental mapping of the catalyst was obtained by scanning electron

microscopy coupled to energy dispersive spectroscopy (SEM-EDS) using a Zeiss microscope (20 kV).

3.4 Catalyst performance test

3.4.1 RWGS reaction

In each experiment, a fresh (as prepared) catalyst was first reduced at 250 °C under a flow of H_2 (200 ml/min) for 1 h. Catalytic performance was evaluated in terms of CO_2 conversion and selectivity to CO production over the range of temperatures (250-500 °C) and space velocities. The gas hourly space velocity (GHSV) is calculated as follows (Q_f is the volumetric feed flow rate and W_c is the catalyst weight):

$$GHSV = \frac{Q_f}{W_c} \tag{6}$$

CO_2 conversion and CO selectivity were calculated using Eq. (7) and Eq. (8), correspondingly (y_{CO_2}, y_{CO}, and y_{CH_4} are mole fractions measured by the IR analyzer on dry basis, i.e., after removal of condensed water and humidity as explained above, Figure 6):

$$X_{CO_2} = \frac{y_{CO} + y_{CH_4}}{y_{CO_2} + y_{CO} + y_{CH_4}} \tag{7}$$

$$S_{CO} = \frac{y_{CO}}{y_{CO} + y_{CH_4}} \tag{8}$$

Carbon balance is defined as the total rate of carbon fed to the reactor divided by the rate of carbon exiting the reactor, as defined by the following equation:

$$CB = (y_{CO_2} + y_{CO} + y_{CH_4})(1 + \alpha - f_1 - 4f_2) \tag{9}$$

In Eq. (9), α, f_1, and f_2 stand for H_2:CO_2 ratio in the feed, conversion to CO, and conversion to CH_4, as defined in Eqs (9a-c) below ($F_{C,out}$ is the total outlet carbon-based molar flow rate):

$$\alpha = \frac{F_{H_2,f}}{F_{CO_2,f}} \tag{9a}$$

$$f_1 = \frac{y_{CO}}{y_{CO} + y_{CO_2} + y_{CH_4}} \equiv \frac{F_{CO,out}}{F_{C,out}} = \frac{F_{CO,out}}{F_{CO_2,f}} \tag{9b}$$

$$f_2 = \frac{y_{CH_4}}{y_{CO} + y_{CO_2} + y_{CH_4}} \equiv \frac{F_{CH_4,out}}{F_{C,out}} = \frac{F_{CH_4,out}}{F_{CO_2,f}} \tag{9c}$$

Eq. (9) above is obtained from the carbon balance definition, Eq. (9d), using Eqs (9a-c) and Eq. (9e) to define the total outlet molar flow rate ($F_{CO,out}$ and $F_{CH_4,out}$ in Eq. (9e) correspond to the H_2 consumption in the RWGS and Sabatier reactions, Eqs (1, 2)):

$$CB = \frac{(y_{CO_2} + y_{CO} + y_{CH_4})F_{t,out}}{F_{CO_2,f}} \tag{9d}$$

$$F_{t,out} = F_{CO_2,f} + F_{H_2,f} - F_{CO,out} - 4F_{CH_4,out} \tag{9e}$$

Carbon balance was continuously monitored and recorded in all experiments (using LabVIEW). Deviations did not exceed 5% in all experiments, i.e., the carbon balance was in the *CB = 0.95-1.05* range.

3.4.2 Biogas/Landfill gas direct upgrade

Catalytic performance was evaluated in the range of temperatures of T=350-600 °C with space velocities ranging from GHSV = 90,000-420,000 mL/(g h). The CH_4-to-CO_2 feed ratio was kept at CH_4:CO_2 = 1 in all tests. In most experiments (specified in the text if otherwise), the H_2-to-CO_2 feed ratio was H_2:CO_2 = 4. Pressure was kept at 3 bars in all experiments. CO_2 conversion (X_{CO_2})

and CH_4 selectivity (S_{CH_4}) were obtained from the following equations (y_{CO_2}, y_{CO}, and y_{CH_4} are mole fractions measured by the IR analyzer on dry basis):

$$X_{CO_2} = \frac{y_{CO} + y_{CH_4} - \beta(y_{CO} + y_{CO_2} + y_{CH_4})}{(1-\beta)(y_{CO} + y_{CO_2} + y_{CH_4})} \tag{10}$$

$$S_{CH_4} = \frac{y_{CH_4} - \beta(y_{CO} + y_{CO_2} + y_{CH_4})}{y_{CO} + y_{CH_4} - \beta(y_{CO} + y_{CO_2} + y_{CH_4})} \tag{11}$$

To obtain Eqs (10, 11), CO_2 conversions to CO, Eq. (12), and to CH_4, Eq. (13) are first defined:

$$f_3 = \frac{y_{CO}}{(1-\beta)(y_{CO} + y_{CO_2} + y_{CH_4})} \equiv \frac{F_{CO,out}}{F_{CO_2,f}} \tag{12}$$

$$f_4 = \frac{y_{CH_4} - \beta(y_{CO} + y_{CO_2} + y_{CH_4})}{(1-\beta)(y_{CO} + y_{CO_2} + y_{CH_4})} \equiv \frac{F_{CH_4,gen}}{F_{CO_2,f}} \tag{13}$$

β is the CH_4 content in the carbon-based feed, as defined in Eq. (14):

$$\beta = \frac{F_{CH_4,f}}{F_{CH_4,f} + F_{CO_2,f}} = \frac{F_{CH_4,f}}{F_{C,f}} \tag{14}$$

The total CO_2 conversion and CH_4 selectivity are then obtained as follows:

$$X_{CO_2} = f_3 + f_4 \tag{10a}$$

$$S_{CH_4} = \frac{f_4}{f_3 + f_4} \tag{11a}$$

Carbon balance (CB) is defined as the total rate of carbon fed to the reactor divided by the rate of carbon exiting the reactor:

$$CB = (y_{CO_2} + y_{CO} + y_{CH_4})(1 + \alpha - f_3 - 4f_4 + \gamma)(1-\beta) \tag{15}$$

In Eq. (15), the feed H_2:CO_2 ratio (α) and feed CH_4:CO_2 ratio (γ) are defined as follows:

$$\alpha = \frac{F_{H_2,f}}{F_{CO_2,f}} \tag{15a}$$

$$\gamma = \frac{F_{CH_4,f}}{F_{CO_2,f}} \tag{15b}$$

To obtain Eq. (15), the carbon balance definition, Eq. (15c), is expressed in terms of above-mentioned definitions using the total outlet flow rate $F_{t,out}$ defined by Eq. (15d):

$$CB = \frac{F_{C,out}}{F_{C,f}} = \frac{(y_{CO_2} + y_{CO} + y_{CH_4})F_{t,out}}{F_{CO_2,f} / (1-\beta)} \tag{15c}$$

$$F_{t,out} = F_{CO_2,f} + [F_{H_2,f} - F_{CO,out} - 4(F_{CH_4,out} - F_{CH_4,f})] + F_{CH_4,f} \tag{15d}$$

$F_{CO,out}$ and $F_{CH_4,out}$ in Eq. (15d) correspond to the H_2 consumption in the RWGS and Sabatier reactions, Eqs (1, 2). In all testes conducted carbon balance was monitored and recorded continuously with LabVIEW. Deviations of carbon balance did not exceed 5%, i.e., the carbon balance was in the *CB = 0.95-1.05* range.

Chapter 4
Results and Discussion

4.1 RWGS reaction

4.1.1 Performance

Comparison between the catalytic activity of the Ru-promoted catalyst (0.5wt% Ru-40wt% $Cu/ZnO/Al_2O_3$, denoted as ″Ru-Cu/ZnO″ throughout the text) with the baseline 40wt% $Cu/ZnO/Al_2O_3$ (denoted as ″Cu/ZnO″ throughout the text) is shown in Figure 7. Error bars show standard deviation between three measurements using different batches of the catalyst. The selectivity to CO production, Eq. (8), was complete ($S_{CO} = 1$) in all measurements reported in Figure 6. For temperatures higher than 400 °C, over 100% improvement of the CO_2 conversion is observed, Figure 7a. At 500 °C, the CO_2 conversion reached 46%, whereas the corresponding equilibrium conversion is 55%. For the baseline Cu/ZnO catalyst, only 17% conversion was achieved at 500 °C. Therefore, the Ru promotion results in a substantial improvement of the catalyst activity. The intriguing observation was that the Ru-Cu/ZnO catalyst did not produce any CH_4, although it is well known that Ru is an excellent methanation catalyst [57]. This finding is investigated in next part.

As GHSV is increased (Figure 7b), the CO_2 conversion expectably decreases due to shorter contact times. Selectivity to CO production was complete (no CH_4 formation) over the entire GHSV range for both catalysts. While for the baseline Cu/ZnO catalyst conversion drops below 10% for space velocities higher than 100,000 mL/(g h), the Ru-Cu/ZnO catalyst maintain conversions ranging 20-30% over the 100,000-200,000 mL/(g h) range. For GHSV > 50,000 mL/(g h), the CO_2 conversion improvement of more than 100% is achieved as compared to the baseline

Cu/ZnO catalyst. Note that for the Ru-Cu/ZnO catalyst the CO_2 conversion approaches 45% at GHSV = 20,000 mL/(g h) which corresponds to the industrially relevant residence time of ~ 150 ms. The effect of the feed H_2/CO_2 ratio is shown in Figure 7c. Complete CO selectivity was obtained over the entire space velocity range for both catalysts. As expected, conversion increases for higher H_2/CO_2 feed ratios, with the CO_2 conversion improvement over 100% for the Ru-Cu/ZnO catalyst as compared to the baseline. As it can be seen from analyzing Figure 7a, the CO_2 conversion improvement increases in a highly nonlinear way as a function of temperature. The improvement dependence on GHSV and H_2:CO_2 is weaker, which may indicate that the addition of Ru affects the apparent activation energy of the catalyst. Recall that only 0.5wt% Ru was added while the main active phase content was 40wt% Cu, i.e., the Ru content was 1.2% of the total active phase.

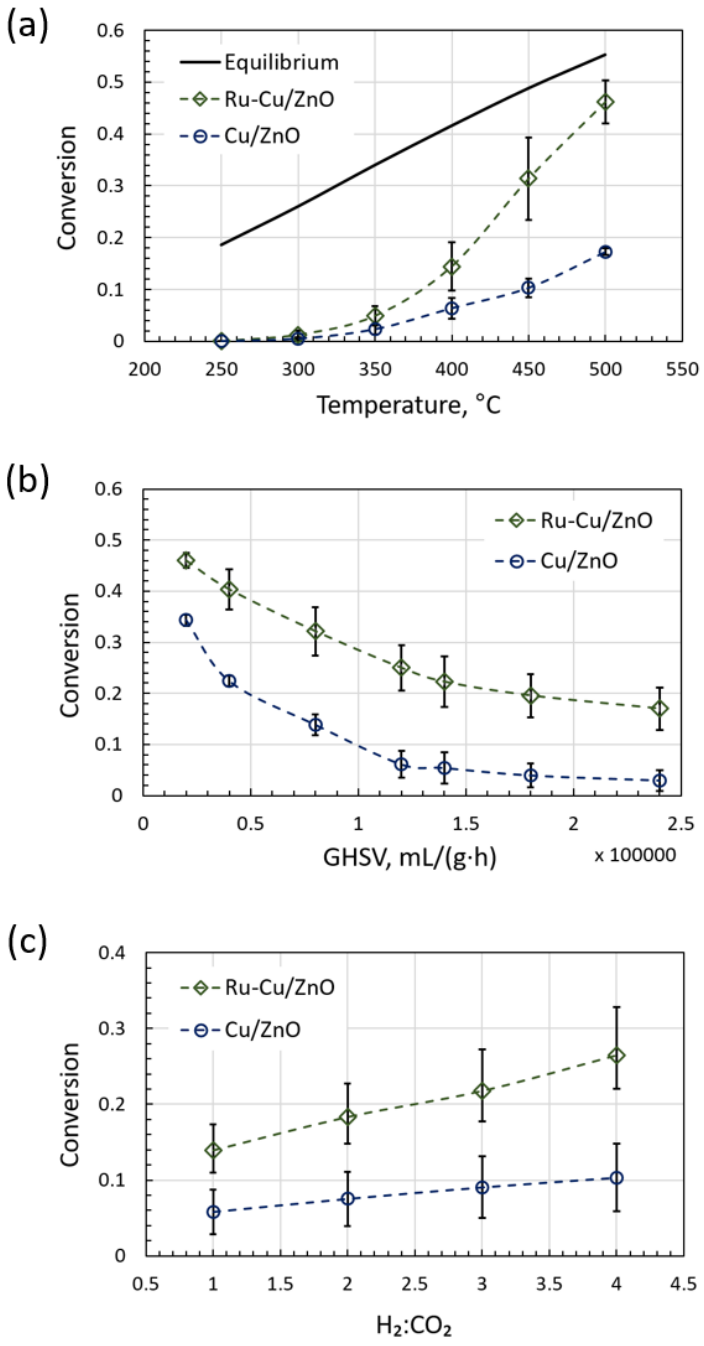

Figure 7. Performance comparison of the 40wt% $Cu/ZnO/Al_2O_3$ and 0.5wt% Ru-40wt% $Cu/ZnO/Al_2O_3$ catalysts. CO_2 conversion is shown as a function of temperature (a), space velocity (b), and feed H_2:CO_2 ratio (c). Parameters: P = 45 psi, GHSV = 90,000 mL/(g h) (a, c), T = 450 °C (b, c), H_2:CO_2 = 4 (a, b).

As it was shown in Figure 7, no CH_4 production was detected when Ru was added to the Cu/ZnO catalyst, although it is well known that Ru is highly active in CO_2 methanation [13,51,58]. While the characterization results (Section 5.1) provided some insight regarding enhanced activity and stability, the origin of the complete selectivity to CO production remained unclear. In order to investigate this finding, Cu and ZnO were gradually removed from the catalyst formulation, while keeping same preparation procedure (as described in Section 3.1), Figure 8. Removal of Cu (denoted as Ru/ZnO in Figure 8) resulted in a significant drop in catalytic activity but the selectivity to CO production remained complete, with no CH_4 formation detected while scanning vs. temperature and GHSV, Figure 8. The most interesting observation from this experiment is that the 0.5 wt% $Ru/ZnO/Al_2O_3$ catalyst acts as a RWGS catalyst exclusively selective to CO formation.

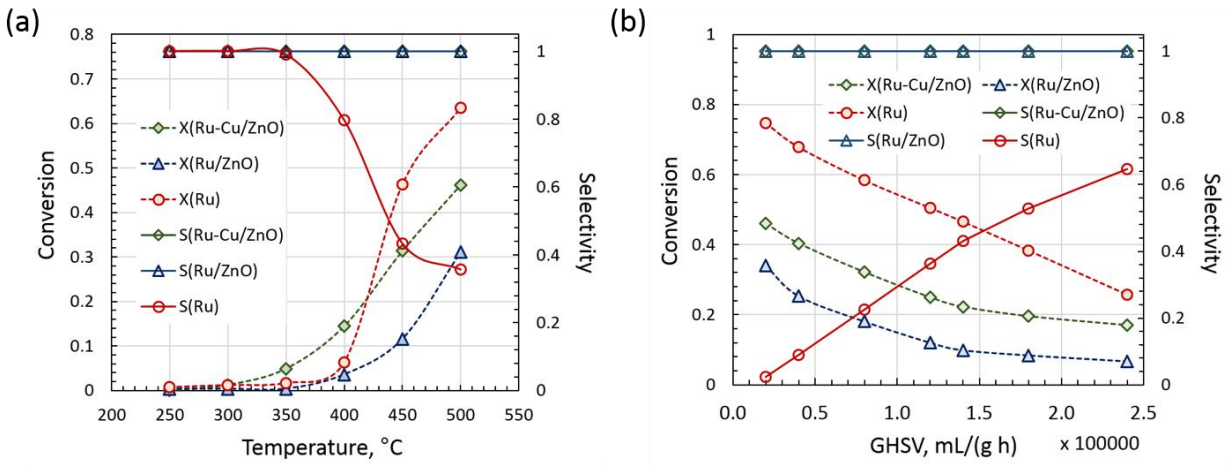

Figure 8. Catalytic performance evaluation of the $Ru\text{-}Cu/ZnO/Al_2O_3$, $Ru\text{-}ZnO/Al_2O_3$ and Ru/Al_2O_3 catalysts vs. temperature (a) and space velocity (b). Parameters: P = 45 psi, H_2:CO_2 = 4, GHSV= 100,000 mL/(g h) (a), T = 450 °C (b).

Only after removing ZnO the Ru/Al_2O_3 catalyst (denoted as Ru in Figure 8) produced both CO and CH_4 with the CO selectivity dropping below 40% at 500 °C (Figure 8a). The CO_2 conversion

of that catalyst actually increased to 63% at 500 °C due to CH_4 formation. The CO_2 conversion of the Ru/Al_2O_3 catalyst was much higher as compared to other formulations when scanned over the range of space velocities, Figure 8b, with a nearly complete selectivity to CH_4 formation at relatively low space velocities. Altogether these findings indicate that the interaction between Ru and ZnO could be necessary for CH_4 formation suppression.

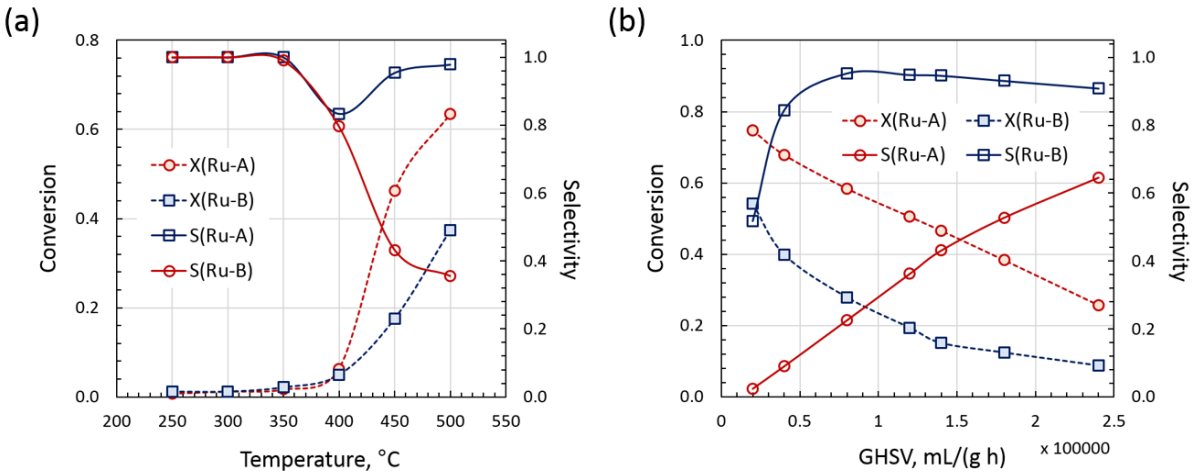

Figure 9. Catalytic performance evaluation of the Ru/Al_2O_3 catalysts prepared by Ru impregnation on the uncalcined alumina (A) and calcined alumina (B). P = 30 psi, H_2:CO_2 = 4, GHSV = 100,000 mL/(g h) (a), T = 450 °C (b).

To investigate the importance of the Ru-Al_2O_3 interaction, an additional Ru-Al_2O_3 sample was prepared using a pre-calcined Al_2O_3 support for impregnation (see Section 3.1 for details). The comparison between two samples is shown in Figure 9. It can be clearly seen that the Al_2O_3 support pre-treatment had a very significant effect on both CO_2 conversion and CO selectivity. Calcining the support prior to impregnation resulted in lower conversion but higher selectivity to CO formation, attaining ~ 95% CO selectivity at high temperatures and space velocities. This observation is important as it indicates that it is possible to control the Ru selectivity by modifying the support structure even using same support material (Al_2O_3).

4.1.2 Stability

Catalyst stability is an important aspect of catalytic performance often overlooked in laboratory studies. As the $Cu/ZnO/Al_2O_3$ catalyst is known to deactivate rapidly in methanol synthesis [59], its stability in the RWGS reaction could be also poor. Stability tests were conducted for the baseline Cu/ZnO catalyst as well as for the promoted Ru-Cu/ZnO catalyst, Figure 10. For the Cu/ZnO catalyst the stability was relatively good at 450 °C, achieving the CO_2 conversion of 30% in the beginning of operation with a decline to nearly 20% over 70 h on stream, Figure 10a. However, for practical applications significantly higher temperatures will be required to achieve reasonably high conversions. At 700 °C, the initial conversion was 70% for the Cu/ZnO catalyst, Figure 10a. However, the catalyst bed was completely clogged after 25 h on stream at that temperature as it was evident from increasing the reactor outlet pressure followed by the feed flow stoppage, which corresponds to the sharp failure recorded in Figure 10a.

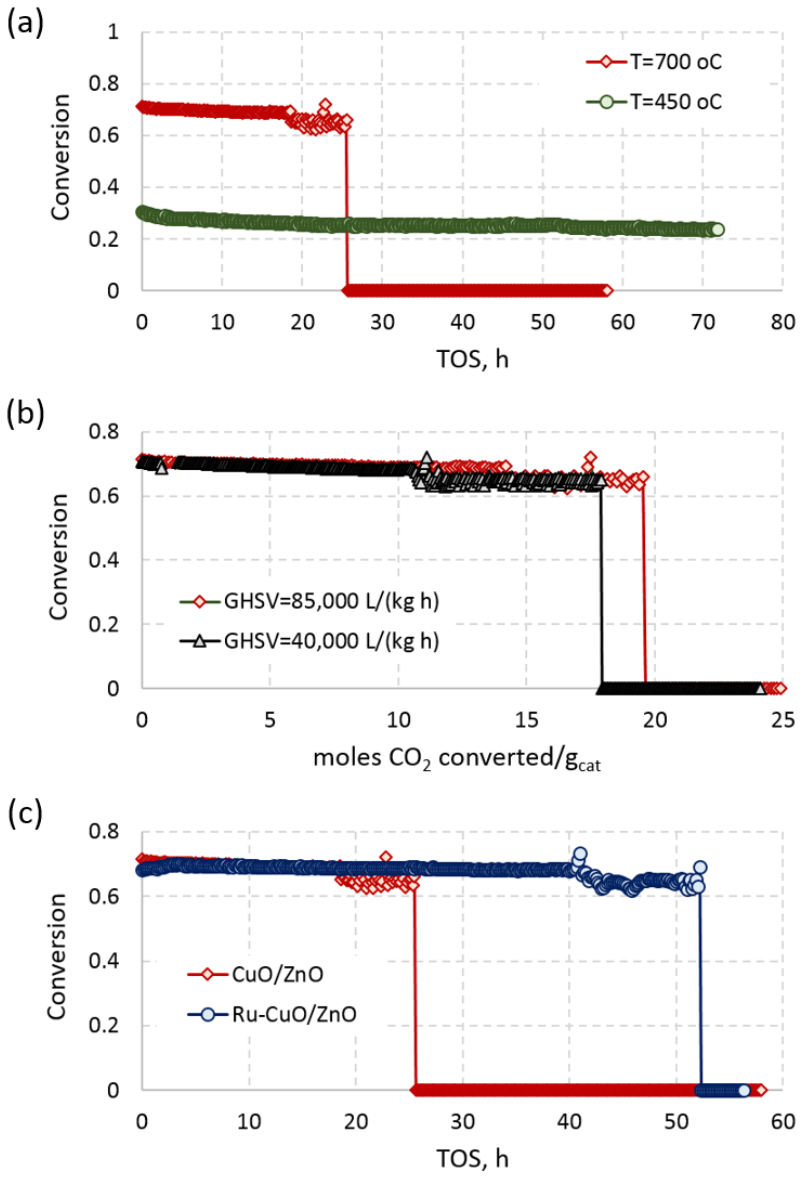

Figure 10. Catalyst stability comparison (CO_2 conversion vs. time on stream (TOS), (a, c) and amount of converted CO_2 (b)): (a) Cu/ZnO performance at 450 °C and 700 °C at GHSV = 85,000 mL/(g h); (b) Cu/ZnO performance at 700°C for GHSV = 40,000 and 85,000 mL/(g h); (c) comparison between the Ru-Cu/ZnO and Cu/ZnO catalysts at 700 °C and GHSV = 85,000 mL/(g h). Other parameters: P = 45 psi, H_2:CO_2 = 4. Selectivity to CO formation was 100% for all data reported in Figure 10.

In order to investigate the reason for this failure, two additional stability tests were conducted at 700 °C and two different space velocities, as it is shown in Figure 10b, where the CO_2 conversion is plotted vs. number of moles of converted CO_2 per gram of catalyst. Reactor clogging and failure happened faster for higher space velocity, but for similar amount of converted CO_2. This observation indicates that the mechanism of catalyst failure is coking rather than sintering, as the rate of sintering (which is induced by temperature) should not be correlated with the amount of converted CO_2. With Ru promotion, reactor failure occurred after more than 50 h as compared to 25 h observed for the Cu/ZnO catalyst under identical conditions, Figure 10c. For all stability tests performed at 700 °C, Figure 10, same catalyst failure pattern was observed: initial slow rate of deactivation followed by a relatively small conversion drop and fluctuations, which were associated with the catalyst bed resistance build up (pressure increase at the reactor outlet), with eventual abrupt failure when the outlet pressure was equal to the feed pressure causing the feed flow stoppage, i.e., pressured drop buildup in the catalytic bed.

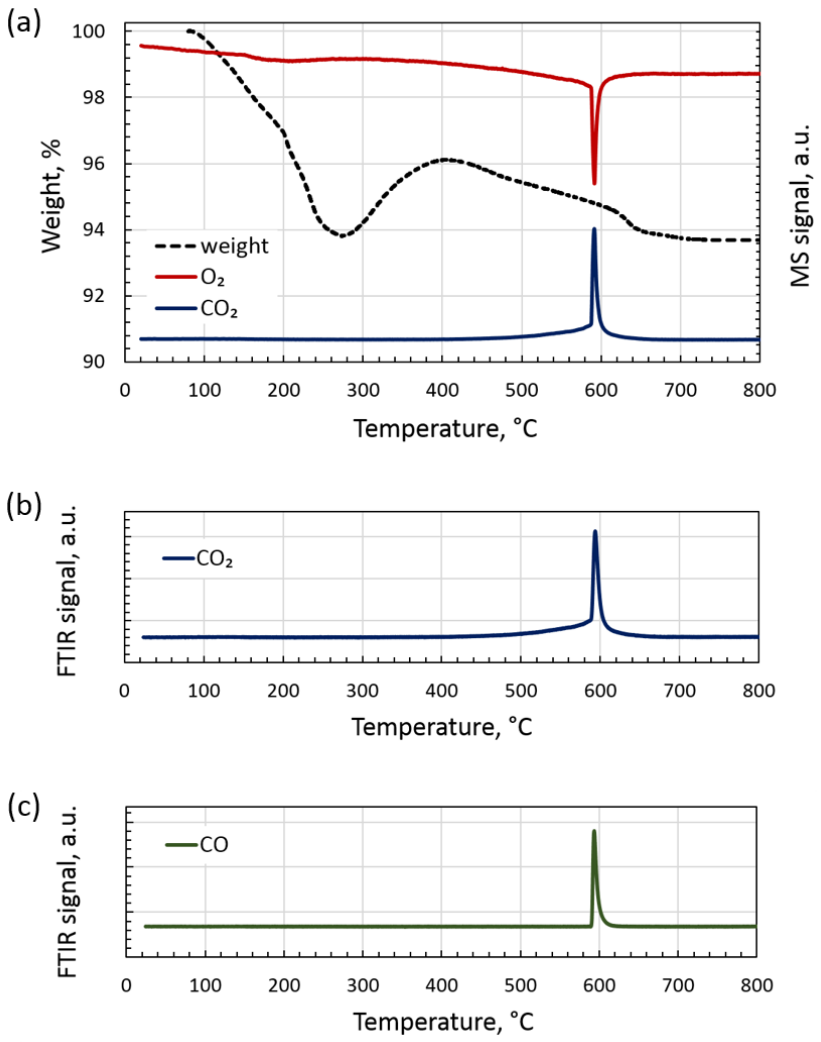

Figure 11. TGA-TPO test of the spent $Cu/ZnO/Al_2O_3$ catalyst ran at 700 °C, showing TGA-MS (a) and FTIR (b, c) signals. Temperature ramping rate was 10 °C/min for T ≤ 150 °C and 2 °C/min for T = 150-800 °C. Air flow rate was 40 ml/min.

The observed catalyst bed failure pattern indicated the possibility of strong coking, which can eventually lead to the catalyst clogging by deposited carbon. To test this hypothesis, thermal gravimetric analysis (TGA) combined with temperature programmed oxidation (TPO was performed on the spent Cu/ZnO catalyst obtained after the reactor failure shown in Figure 10. TGA-TPO signals are shown in Figure 11. There is an initial weight drop of ~ 6% for T < 250 °C

which can be associated with the water desorption from the sample, Figure 11a. For T = 280-400 °C, the sample weight increases by ~2% and then decreases by similar amount over T = 400-700 °C. The weight increase can be associated with Cu oxidation, while the weight loss should be attributed to the deposited carbon oxidation, as it is evident from CO_2 and CO signals detected by both MS (Figure 11a) and FTIR (Figure 11b, c). The consumption of O_2 is also evident from the MS signal, Figure 11a; it starts as a gradual decline at ~ 280 °C with a sharp peak at 590 °C clearly associated with the sharp peaks of CO_2 and CO release. From the analysis of Figures 10, 11, it can be concluded that the reason for reactor failures was accumulation of the deposited carbon followed by complete clogging of the catalyst. Although the addition of Ru improves the catalyst resistance against coking significantly, same type of failure was observed for the Ru-promoted catalyst. On the other hand, no reactor clogging was observed over similar time on stream (70 h) at 450 °C, Figure 10a. As no CH_4 formation was observed, the source of carbon formation should be CO (Eqs. 4, 5), which coincides with the fact that faster deactivation was observed at higher CO_2 conversions (CO is a product in the RWGS reaction).

4.2 Biogas/Landfill gas direct upgrade

4.2.1 Performance

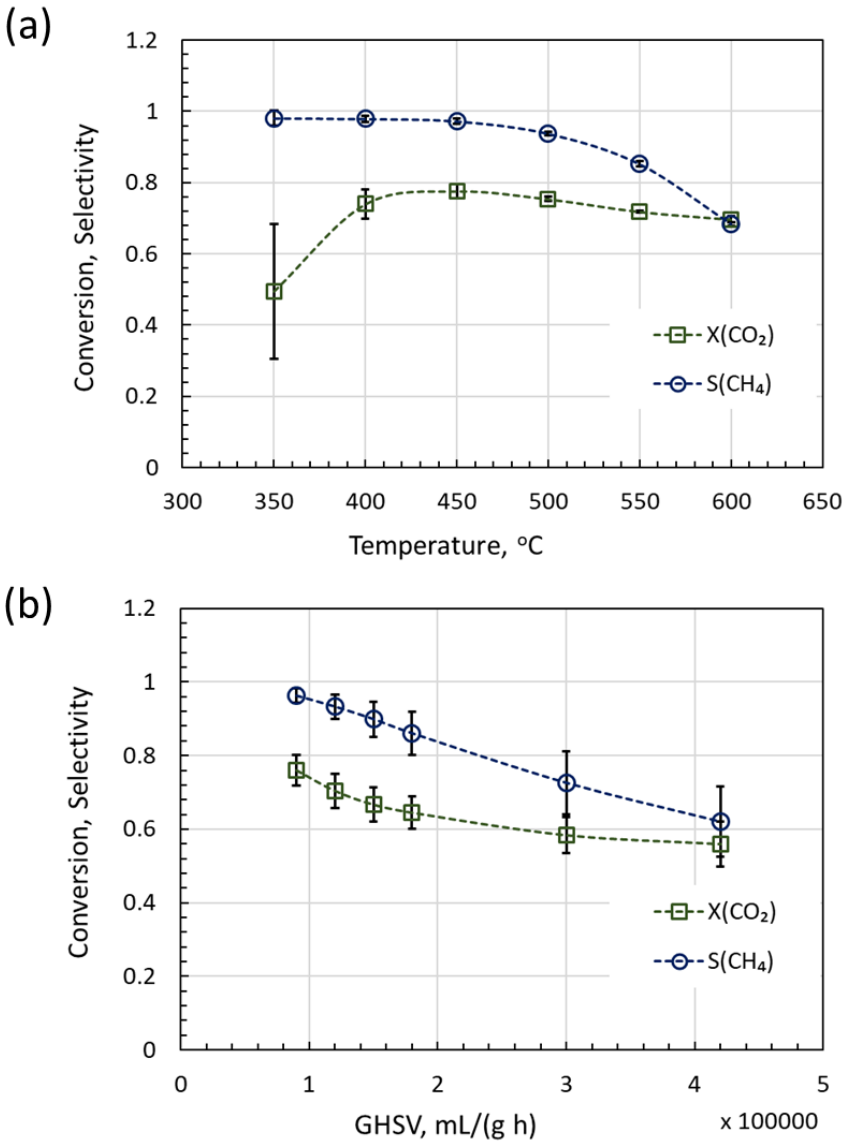

Figure 12. Performance of the 0.5wt% Ru/Al_2O_3 as a function of (a) temperature and (b) GHSV. Parameters: (a) GHSV = 90,000 mL/(g h), H_2:CO_2 = 4, CH_4:CO_2 = 1, P = 3 bar, (b) T = 450 °C, H_2:CO_2 = 4, CH_4:CO_2 = 1, P=3 bar.

The performance of the 0.5wt% Ru/Al_2O_3 catalyst as a function of temperature and gas hourly space velocity (GHSV) is shown in Figure 12. Error bars show standard deviation between three separate measurements obtained with different catalyst batches: good repeatability between different data sets were obtained. At 350-450 °C, CH_4 selectivity is nearly 100% followed by a gradually decrease to 65% at 600 °C. The CO_2 conversion increases from 50% at 350 °C to nearly 80% at 450 °C, with a small decline to 70% at 600 °C. The observed decline in selectivity is in line with the fact that methanation and RWGS reactions are exothermic and endothermic, respectively, Eqs. (1-3), so that more CO is produced at higher temperature.

Effect of GHSV is shown in in Fig. 12b: both CO_2 conversion and CH_4 selectivity decline with increasing space velocity. The conversion decline for higher space velocities is expected because of shorter contact times. The nearly linear selectivity decline is probably related to different reaction rate scales of RWGS and methanation, i.e., if the RWGS rate is faster, it will be less affected by shorter contact times, resulting in higher selectivity to CO formation. From a practical point of view, in order to keep high CH_4 selectivity GHSV should be kept relatively low space velocity (less than 100,000 mL/(g h). Note that GHSV = 100,000 mL/(g h) corresponds to a residence time of ~ 50 ms, thus even operating at GHSV = 10,000 mL/(g h) can be considered as industrially relevant (residence time on an order of magnitude of 1 s).

Catalyst performance as a function of the feed H_2:CO_2 ratio and operating pressure is shown in Figure 13. Though neither H_2:CO_2 ratio nor pressure have as strong effect as temperature and GHSV, both CO_2 conversion and CH_4 selectivity were improved by ca. 20%, which is important for practical applications. From the thermodynamic point of view, both pressure and excess H_2 favor methanation reactions, Eqs (2, 3). At H_2:CO_2 = 4.5, the CO_2 conversion and CH_4 selectivity reach 85% and 97%, respectively, Figure 13a. As it can be seen in Figure 13b, the increase of

pressure from 3 to 3.75 bar, results in only minor improvement. In all results reported beyond this point, the reactor pressure was maintained at 3 bar.

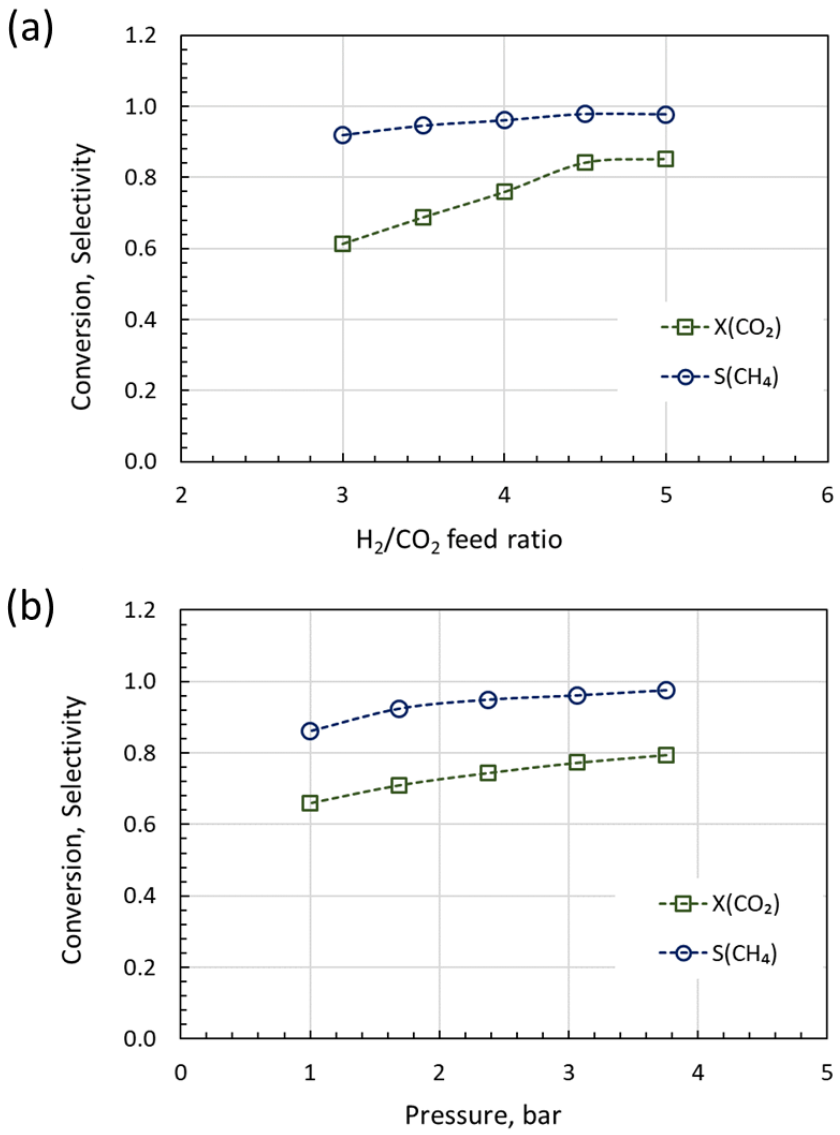

Figure 13. Performance of the 0.5wt% Ru/Al_2O_3 as a function of H_2:CO_2 ratio (a) and pressure (b). Parameters: T = 450 °C, GHSV = 90,000 mL/(g h), CH_4:CO_2 = 1, P=3 bar (a), and H_2:CO_2 = 4 (b).

Although Ru is the least expensive noble metal, its cost is expected to be among the major drawbacks in large-scale implementation. To identify the lowest possible Ru loading, a series of catalysts with the Ru loading ranging from 0.05-1wt% were tested. Catalytic performance was evaluated in terms of CO_2 conversion and selectivity to CH_4 production over the range of temperatures (Figure 14) and space velocities (Figure 15). Lowering the Ru loading results in lower CO_2 conversions, with the difference being more pronounced at the low temperature range (350-450 °C). However, at 550-600 °C all catalysts showed very similar performance.

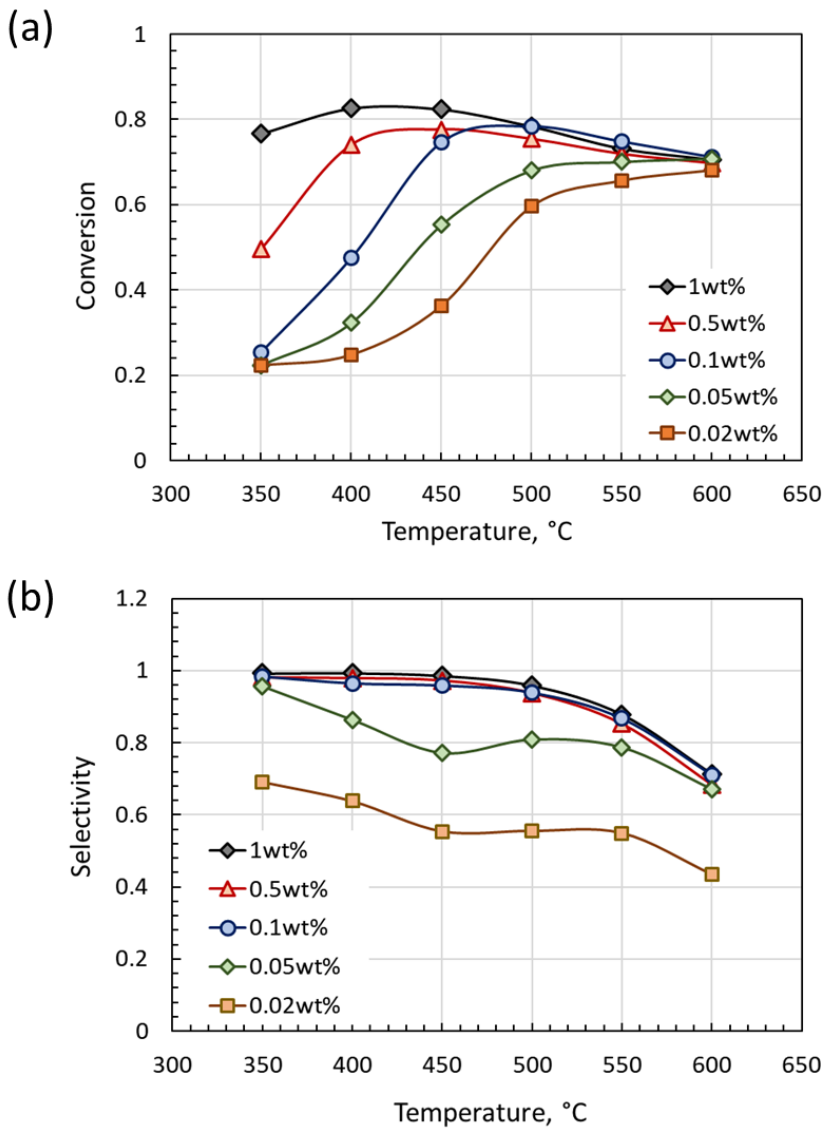

Figure 14. CO_2 conversion (a) and CH_4 selectivity (b) of the 0.05-1wt% Ru/Al_2O_3 catalysts as a function of temperature. Reaction condition: GHSV = 90,000 mL/(g h), H_2:CO_2 = 4, CH_4:CO_2 = 1, P=3 bar.

In terms of CH_4 selectivity, 0.1-1wt% Ru/Al_2O_3 catalysts showed very similar performance over the entire tested temperature range (350-600 °C), Figure 14b. The catalysts with lower loadings (0.05 and 0.02wt% Ru) had significantly lower CH_4 selectivity as compared to higher loadings. This finding is in line with another study reported in the literature, showing a clear

correlation between decreasing Ru loadings (5-0.1wt%) and increasing CO yields (ca. 10-20%) at 400-500 °C [51].

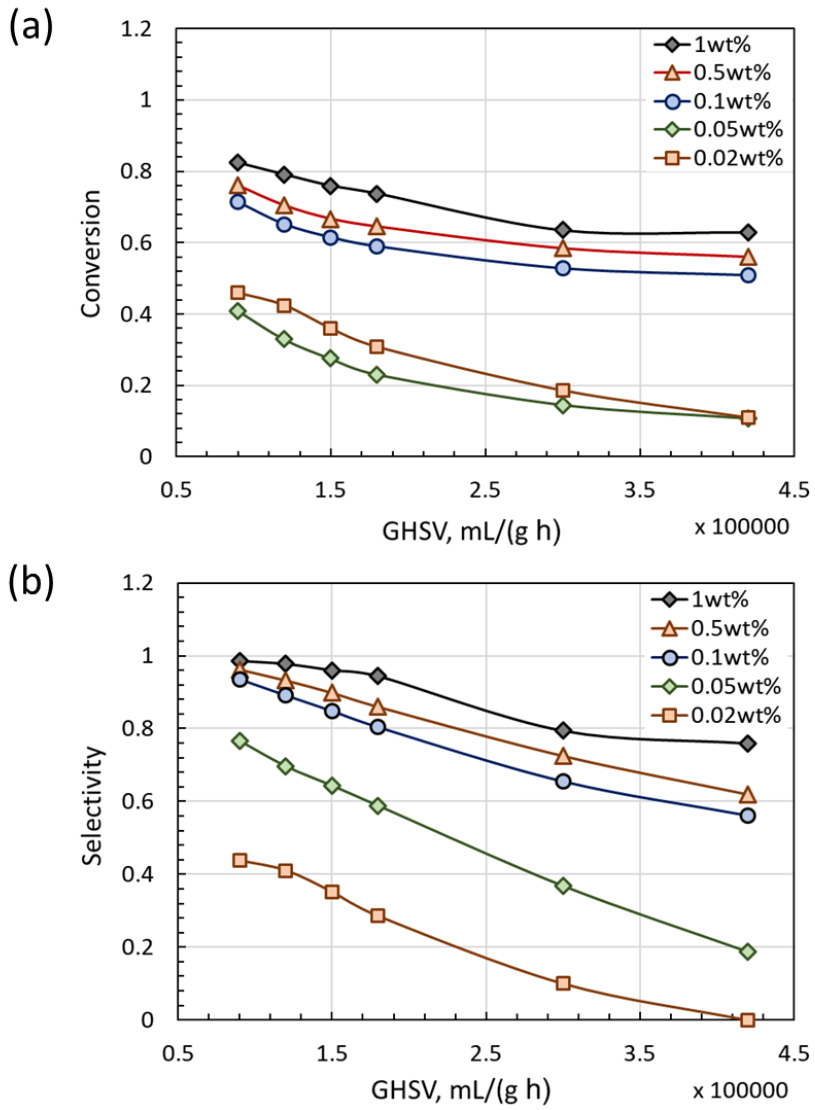

Figure 15. CO_2 conversion (a) and CH_4 selectivity (b) of the 0.05-1wt% Ru/Al_2O_3 as a function of GHSV. Reaction condition: T = 450 °C, H_2:CO_2 = 4, CH_4:CO_2 = 1, P=3 bar.

CO_2 conversion and CH_4 selectivity as a function of GHSV are shown in Figure 15. In terms of CO_2 conversion, Figure 15a, all catalysts tested could be divided into two distinct groups: higher performance (0.1-1wt% Ru) and lower performance (0.02-0.05wt% Ru). While all catalysts

showed similar trends of declining conversion, the CO_2 conversion for the 0.02, 0.05wt% Ru loading was significantly lower (ca. 10-40% over the tested GHSV range as compared to ca. 50-80% for higher loadings). It is interesting that there is no sharp conversion drop for the 0.1-1wt% Ru loadings over the GHSV = 150,000-400,000 mL/(g h) range, which indicates that these catalysts are highly active. The effect of Ru loading on the selectivity to CO production is even more pronounced, Figure 15b. For the 0.1-1wt% Ru loading, the CO selectivity decline follows similar trend as for the CO_2 conversion. For lower Ru loadings, the CO selectivity drops rapidly from 80% to 20% for 0.05wt% and from 40% to 0% for 0.02wt% over the tested GHSV range.

4.2.2 Stability

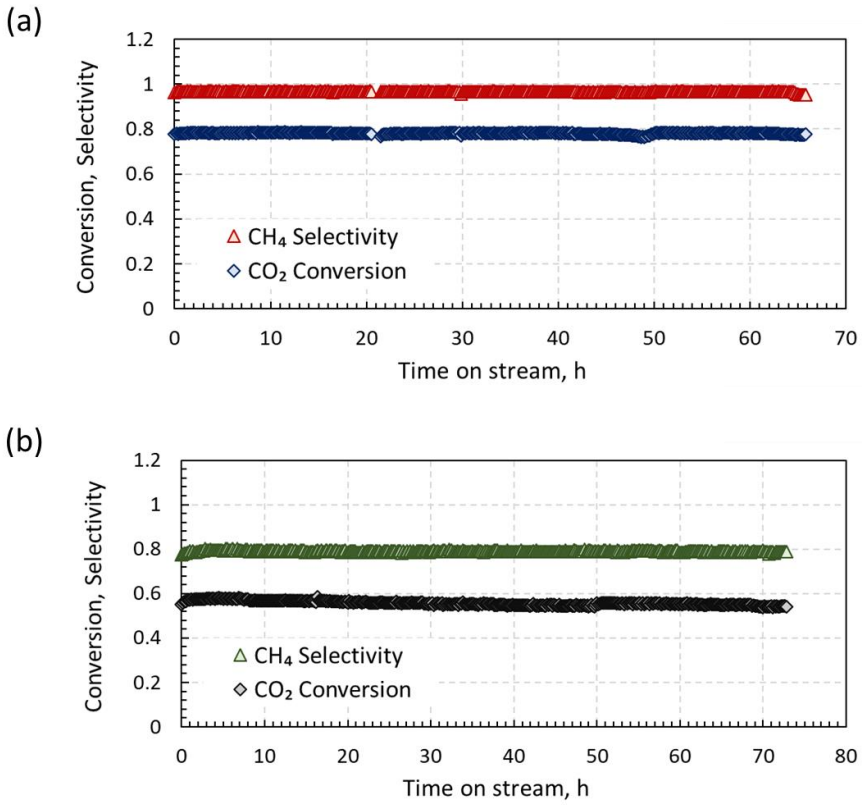

Figure 16. Stability comparison of the 0.5wt% (a) and 0.05wt% (b) Ru/Al_2O_3. Operating conditions: P = 3 bar, T = 450 °C, GHSV = 90,000 mL/(g h), H_2:CO_2 = 4.

Catalyst stability is an important aspect of catalytic performance often overlooked in laboratory studies. There are three major pathways for catalyst deactivation, namely poisoning, sintering, and coking [10]. Since the experiments reported herein were conducted with a synthetic mixture not containing any impurities, poisoning is not expected to occur. Sintering is relevant as a deactivation mechanism, as it is induced by temperature. However, CO_2 methanation does not require high temperatures and sintering is not expected to occur to a significant extent at 450 °C, which was the optimal temperature in terms of conversion and selectivity, Figure 12. Coking on the other hand is expected to occur under the methanation reaction conditions [22]. Stability tests for the 0.5wt% and 0.05wt% Ru/Al_2O_3 catalysts are shown in Figure 16. For both no notable deactivation was detected during 60-70 h on stream. Although no deactivation was observed over the tested time interval, carbon deposition may still occur to a certain extent. To investigate the possibility of coking, the spent catalysts were analyzed by TGA-MS, Fig. 17.

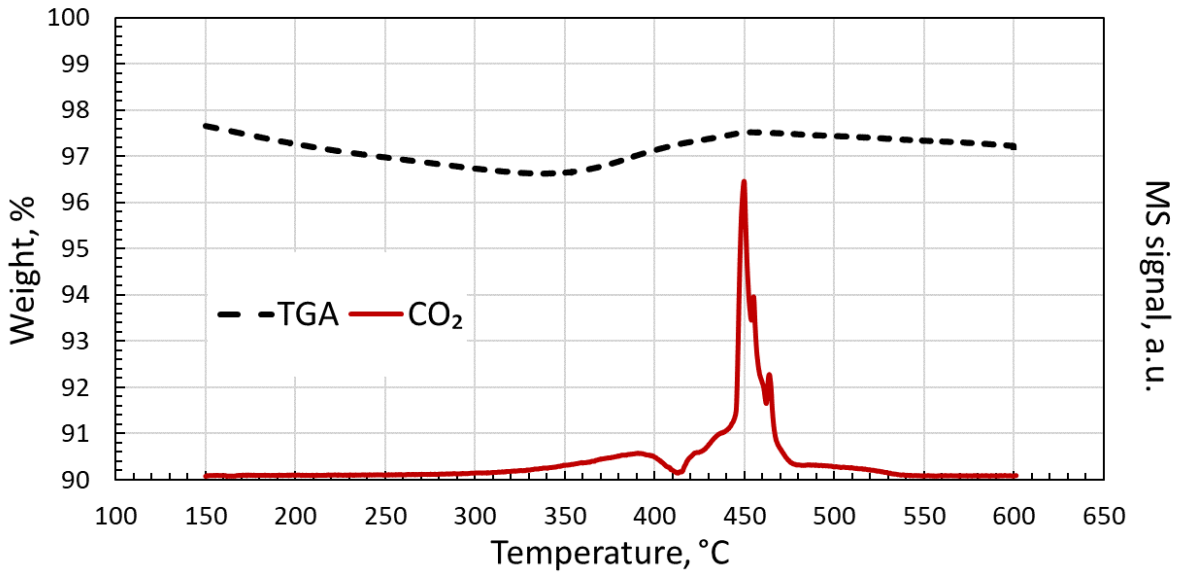

Figure 17. TGA-MS analysis of the spent 0.5wt% Ru/Al_2O_3 catalyst after 70 h on stream at 450 °C. Temperature ramping rate was 10 °C/min for T ≤ 150 °C and 2 °C/min for T = 150-600 °C. Air flow rate was 40 ml/min.

The initial weight loss of 2.3% occurred during the first step of temperature ramp for T < 150 °C (see Section 3.3), due to evaporation of physically adsorbed water. Further weight loss for T = 150-330 °C can be attributed to the removal of chemically bound water. Beyond this point, the weight first increases slightly (probably due to Ru oxidation) and then decreases by ~0.5%. The MS CO_2 signal appears at 300-550 °C as two separated peaks which can be attributed to different types of deposited carbon. The weight gain associated with CO_2 release can be attributed to the combined effect of Ru and C oxidation, which should result in weight gain and loss, correspondingly. In conclusion, although no deactivation was detected, some carbon was deposited on the catalyst surface. However, since the CO_2 release from the spent catalyst during the TPO experiment, Fig. 17, was not associated with any substantial weight loss, the extent of coking was not significant.

Chapter 5
Characterization Results

5.1 Ru-Cu/ZnO catalysts

The catalyst composition was verified using ICP-MS. Deviations from the targeted composition didn't exceed 10%, i.e., the measured Cu content was in the 39-43wt% range, with the target value being 40wt%. The Cu/ZnO and Ru-Cu/ZnO catalysts were characterized by XRD, SEM-EDS, and TEM in order to investigate the effect of Ru addition on the catalyst structure and morphology.

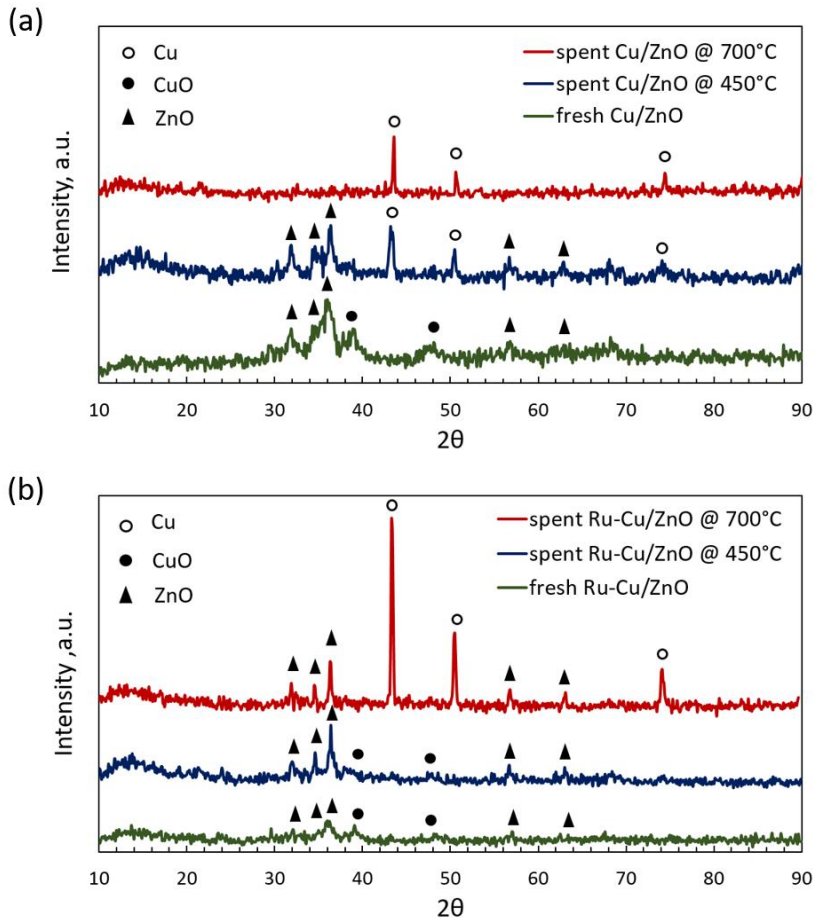

Figure 18. XRD patterns of fresh (as prepared) and spent (after tests at 450 °C and 700 °C) catalysts: (a) $Cu/ZnO/Al_2O_3$(denoted as Cu/ZnO); (b) $Ru\text{-}Cu/ZnO/Al_2O_3$(denoted as Ru-Cu/ZnO).

XRD patterns of fresh and spent catalysts are shown in Figure 18. As expected, CuO and Cu peaks were identified in both catalysts, with Cu peaks being absent in fresh catalysts (as expected) While characteristic peaks of CuO (located at $2\theta = 38.7°$) were found in both fresh catalysts, they also appear for the Ru-Cu/ZnO catalyst tested at 450 °C, but not for the spent Cu/ZnO catalyst tested under identical conditions. On the other hand, while the two sharp peaks associated with reduced Cu ($2\theta = 43.4°, 50.5°$) appear for the Cu/ZnO catalyst tested at both 450 °C and 700 °C, they are absent in the Ru-promoted catalyst tested at 450 °C. Also, the Cu peaks for the spent Ru-Cu/ZnO catalyst tested at 700°C were sharper as compared to the Cu/ZnO catalyst indicating better crystallinity. Another important observation was that the ZnO peaks were not observed for the Cu/ZnO catalyst tested at 700 °C. Altogether, these findings indicate that the Ru phase not only affects somehow the oxidation state of Cu but also interacts with the support.

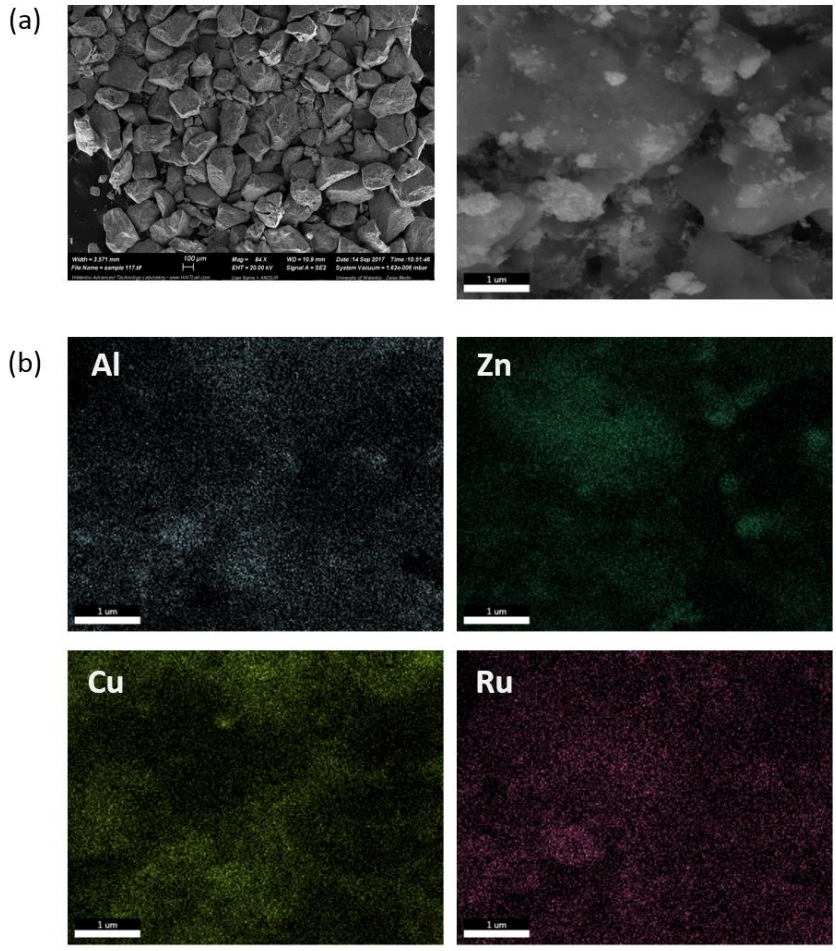

Figure 19. SEM images (a) and elemental mapping (b) of the Ru-Cu/ZnO/Al_2O_3 catalyst. Scale bars are 100 μm for the left micrograph in (a) and 1 μm for other images. Maps in (b) correspond to the right micrograph in (a).

To analyze the dispersion of active phases in the catalyst, SEM-EDS elemental mapping of the Ru-Cu/ZnO catalyst was performed, Figure 19. The mapping showed generally good dispersion of all elements, at least at the microstructural level obtainable with SEM-EDS, Figure 19b (mapping obtained from other location in the same sample showed similar results). Importantly, Ru is well-dispersed throughout the sample. This finding is in line with the results of the catalytic performance evaluation and XRD analysis indicating that Ru does not act as a separate active

phase contributing to the catalyst performance in an additive way. Altogether, these findings indicate that the Ru phase interacts with the Cu phase and the support affecting their performance.

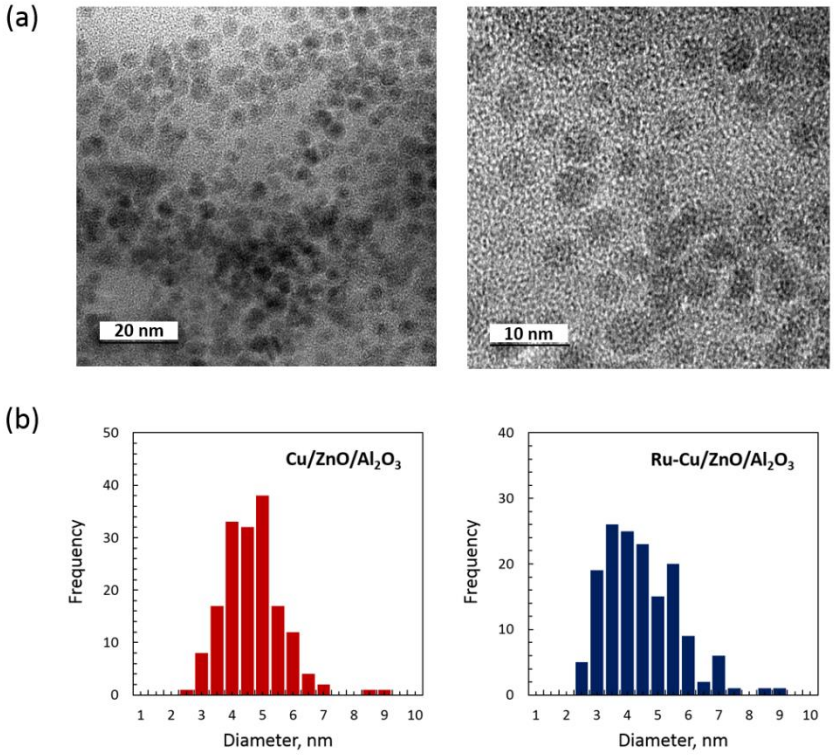

Figure 20. Characteristic TEM micrographs of the spent Cu/ZnO catalyst tested at 450 °C (a) and particle size distributions obtained from analyzing multiple TEM images (b).

TEM images representative of the spent Cu/ZnO and Ru-Cu/ZnO catalysts (tested at 450 °C) are shown in Figure 20a. Round-shaped Cu nanoparticles with particle sizes ranging from 2-9 nm were observed for both catalysts. For the given instrument resolution, it was not possible to identify Ru nanoparticles (total of 5 TEM images were obtained for each catalyst). Particle size distributions (PSDs) acquired from TEM images are show in Figure 20b. For both catalysts, particle size follows nearly normal distribution with the average Cu nanoparticle size of ~4 nm. Therefore, the addition of Ru did not affect the Cu phase dispersion (at least in spent catalysts).

Active phase dispersion was calculated from obtained PSDs using the following equation (accounting for polydispersity):

$$D = \frac{\sum_{i}^{d_{p,\max}} \frac{N_{S,i}}{N_{V,i}} V_{p,i} f_i}{\sum_{i}^{d_{p,\max}} V_{p,i} f_i} = \frac{\sum_{i}^{d_{p,\max}} \frac{\pi d_{p,i}^2}{A_{Me}} \frac{6 M_{W,Me}}{N_A \rho_{Me} \pi d_{p,i}^3} \frac{\pi d_{p,i}^3}{6} f_i}{\sum_{i}^{d_{p,\max}} \frac{\pi d_{p,i}^3}{6} f_i} \tag{16}$$

For a nanoparticle diameter $d_{p,i}$, with the corresponding fraction f_i obtained from a PSD (Figure 20b), $N_{S,i}$ is a number of surface atoms, $N_{V,i}$ is the total number of atoms, and $V_{p,i}$ is the nanoparticle volume. A_{Me} is the surface area occupied by a single active site, N_A is the Avogadro number, ρ_{Me} and $M_{W,Me}$ are the gravimetric density and molecular weight of the active phase. Total 10 TEM images were analyzed counting total 319 particles. Turnover frequency (TOF) was calculated using normalized reaction rates measured under differential conditions (conversion less than 15%):

$$TOF = \frac{M_{W,Me}}{D} R_{max} \tag{17}$$

$$R_{\max} = 100 \frac{r_{\max}}{L_{Me}} \tag{17a}$$

$$r_{\max}(X_{CO_2} < 0.15) = \frac{F_{CO_2,f} X_{CO_2}}{W_c} \tag{17b}$$

L_{Me} is the active phase (Cu) percentage loading, $F_{CO_2,f}$ is CO_2 feed rate, and W_c is the catalyst weight. Results are summarized in Table 1, showing also specific surface area.

Table 1. BET surface area, nanoparticle diameter, dispersion, and TOF for spent catalysts tested at 450 °C.

Catalyst	BET surface area, m^2/g	Diameter, nm	Dispersion	TOF, s^{-1}
$Cu/ZnO/Al_2O_3$	12.9	4.4	0.339	0.011
$Ru\text{-}Cu/ZnO/Al_2O_3$	7.2	4.2	0.335	0.098

The Ru addition resulted in a substantial reduction of the specific surface area, but the Cu phase dispersion was not affected. Therefore, the increase of catalytic activity for the Ru-promoted catalyst was not related to higher specific surface area of the catalyst or better Cu dispersion. Surface area reduced by 45% after the impregnation. On the other hand, the TOF of the Ru-Cu/ZnO catalyst was almost 8 times higher than that for the Cu/ZnO catalyst, Table 1. TOF values reported for other catalysts are ranging from 0.0104 and 0.0998 s^{-1} reported for 1wt% Pt/Al_2O_3 and 1wt% Pt/TiO_2 at 300 °C [14] and 0.428 s^{-1} for Mo_2C at 300 °C [60].

5.2 Ru/Al_2O_3 catalysts

ICP-MS was used to verify that the preparation procedure results in targeted Ru loading. Three separate batches of the 0.5wt% $Ru/\gamma\text{-}Al_2O_3$ catalyst were analyzed and each batch was measured three times, with the obtained standard deviation for both Ru and Al of 0.0011wt%. The average Ru content between three batches was 0.47±0.13 wt%. The BET specific surface area of the 0.5wt% Ru/Al_2O_3 catalyst was 209 m^2/g, as compared to 206 m^2/g for the support before Ru impregnation. Therefore, the Ru impregnation procedure did not affect the surface area significantly.

Chapter 6
Conclusion and Future Work

6.1 RWGS reaction

The RWGS reaction over the 0.5wt% Ru-promoted 40wt% $Cu/ZnO/Al_2O_3$ catalyst was investigated and it was found that the Ru addition resulted in over 100% CO_2 conversion enhancement while maintaining a complete selectivity to CO production. As Ru is known as an excellent methanation catalyst, this finding is intriguing and promising, as it can provide an avenue for controlling the selectivity of catalytic reactions. By gradually removing Cu and ZnO from the catalyst formulation, it was found that Cu is not necessary for CH_4 formation suppression and that 0.5wt% $Ru/ZnO/Al_2O_3$ catalyst is still completely selective to CO formation, although at lower conversion rates. It was also found the Ru selectivity to catalyzing the RWGS and methanation reactions in the absence of ZnO support can be controlled by simple changes in preparation routine. The 0.5wt% Ru/Al_2O_3 can be highly selective to either CO or CH_4 formation depending on Al_2O_3 calcination procedure.

The 0.5wt% Ru-40wt% $Cu/ZnO/Al_2O_3$ catalyst was tested for its catalytic performance over the range of operating conditions: varying temperature, feed H_2/CO_2 ratio, and space velocity, including space velocities as high as 100,000-500,000 mL/(g L) which correspond to residence time of less than 50 ms. Under all conditions tested the catalyst was exclusively selective to CO production, attaining CO_2 conversions as high as 50% at 500 °C and GHSV = 10,000 mL/(g h). The catalyst stability was also significantly improved. However, extensive coke formation was observed at 700 °C.

6.2 Biogas/Landfill gas direct upgrade

In this study, the feasibility of upgrading landfill gas and biogas into renewable natural gas (RNG) over the Ru/γ-Al_2O_3 catalyst with Ru loadings ranging from 0.02-1wt% was investigated. Using a synthetic 50:50 mixture of CO_2 and CH_4 simulating a pre-treated landfill gas (biogas), it was confirmed that it is possible to upgrade this mixture with CO_2 conversions reaching 80%, while maintaining nearly complete selectivity to CH_4 formation (negligible CO production).

From a practical point of view, this result indicates that it might be possible to convert landfill gas (biogas) to an upgraded mixture containing 50% CH_4, 10% CO_2, and 40% H_2 (for 80% CO_2 conversion and 100% CH_4 selectivity). After downstream H_2 separation (H_2 can be recycled), the upgraded gas will contain 83 vol% CH_4 and 17 vol% CO_2. Typical CH_4 concentration in fossil natural gas are ranging from 87-96 vol% [61]. Therefore, even for 80% CO_2 conversion, the upgraded biogas/landfill gas almost meets the quality of natural gas in terms of CH_4 concentration. Further enhancement of the CO_2 conversion, which could be probably achieved by lowering space velocity below 90,000 mL/(g h) (the minimum space velocity tested in the data reported herein), will result in higher CH_4 enrichment.

The optimal temperature in terms of both CO_2 conversion and CH_4 selectivity was identified as 450 °C. Higher temperatures result in declining CH_4 selectivity due to CO formation via the RWGS reaction (steam CH_4 reforming can potentially contribute to CO formation as well). In terms of active phase loading, 0.1-0.5wt% Ru was identified as an optimal range as these loadings provide high CO_2 conversions and CH_4 selectivity and, at the same time, allow for a significant cost reduction. Below 0.1wt% Ru, both activity and selectivity drop sharply.

Future work should include evaluation of the catalytic performance with more realistic compositions similar to those of landfill gas and biogas, and, ultimately, tests with real samples

collected at landfill gas and biogas facilities. One of the issues to be addressed is the catalyst stability against H_2S poisoning which will determine the acceptable H_2S levels and, thus, the extent of upstream pretreatment. The extent of coking should be also investigated over extended periods of time. Altogether, these future investigations should allow for determination of the feasibility and possible scale of the 0.1-0.5wt% $Ru/\gamma\text{-}Al_2O_3$ catalyst application for renewable natural gas (RNG) production.

Reference

[1] Edenhofer O., et al, 2014: Technical Summary. In: Climate Change 2014: Mitigation of Climate Change. Cambridge University Press, Cambridge, United Kingdom and New York, NY, USA.

[2] Aresta, Michele, and Angela Dibenedetto. "Utilization of CO_2 as a chemical feedstock: opportunities and challenges." Dalton Transactions 28 (2007): 2975-2992.

[3] Manitoba Eco-Network, https://climatechangeconnection.org/emissions/co2-equivalents/, 2016.

[4] Tuinier, Martin J., and Martin van Sint Annaland. "Biogas purification using cryogenic packed-bed technology." Industrial & Engineering Chemistry Research 51.15 (2012): 5552-5558.

[5] Shin, Ho-Chul, et al. "Environmental and economic assessment of landfill gas electricity generation in Korea using LEAP model." Energy Policy 33.10 (2005): 1261-1270.

[6] WBA global bioenergy statistics 2015, World Bioenergy Association, http://www.worldbioenergy.org/uploads/WBA%20Global%20Bioenergy%20Statistics%202015.pdf, 2015.

[7] Centi, Gabriele, and Siglinda Perathoner. "Opportunities and prospects in the chemical recycling of carbon dioxide to fuels." Catalysis Today 148.3 (2009): 191-205.

[8] W. Wang, S. Wang, X. Ma, J. Gong, "Recent advances in catalytic hydrogenation of carbon dioxide. " Chemical Society Reviews 40 (2011) 3703-3727.

[9] S. Perathoner, G. Centi, "CO_2 recycling: A key strategy to introduce green energy in the chemical production chain." ChemSusChem 7 (2014) 1274 – 1282.

[10] D.S.A. Simakov, Renewable Synthetic Fuels and Chemicals from Carbon Dioxide, Springer International Publishing 2017.

[11] B. Kumar, M. Llorente, J. Froehlich, T. Dang, A. Sathrum, C.P. Kubiak, "Photochemical and photoelectrochemical reduction of CO_2." Annual Review of Physical Chemistry 63 (2012) 541-569.

[12] Y. Chen, N.S. Lewis, C. Xiang, "Operational constraints and strategies for systems to effect the sustainable, solar-driven reduction of atmospheric CO_2." Energy Environment Science 8 (2015) 3663-3674.

[13] Garbarino, Gabriella, et al. "Methanation of carbon dioxide on Ru/Al_2O_3 and Ni/Al_2O_3 catalysts at atmospheric pressure: Catalysts activation, behaviour and stability." International Journal of Hydrogen Energy 40.30 (2015): 9171-9182.

[14] Y.A. Daza, J.N. Kuhn, "CO_2 conversion by reverse water gas shift catalysis: comparison of catalysts, mechanisms and their consequences for CO_2 conversion to liquid fuels." RSC Advances 6 (2016) 49675-49691.

[15] M.D. Porosoff, B. Yan, J.G. Chen, "Catalytic reduction of CO_2 by H_2 for synthesis of CO, methanol and hydrocarbons: challenges and opportunities." Energy & Environmental Science. 9 (2016) 62-73.

[16] Mallapragada, Dharik S., et al. "Sun-to-fuel assessment of routes for fixing CO_2 as liquid fuel." Industrial & Engineering Chemistry Research 52.14 (2013): 5136-5144.

[17] Oshima, Kazumasa, et al. "Low temperature catalytic reverse water gas shift reaction assisted by an electric field." Catalysis Today 232 (2014): 27-32.

[18] Bustamante, Felipe, et al. "Kinetic study of the reverse water gas shift reaction in high-temperature, high pressure homogeneous systems." Fuel Chem. Div. Preprints 47 (2002): 663-664.

[19] Rönsch, Stefan, et al. "Review on methanation–From fundamentals to current projects." Fuel 166 (2016): 276-296.
[20] Rostrup-Nielsen, J. R., Karsten Pedersen, and J. Sehested. "High temperature methanation: Sintering and structure sensitivity." Applied Catalysis A: General 330 (2007): 134-138.
[21] Nguyen, T. T. M., L. Wissing, and M. S. Skjøth-Rasmussen. "High temperature methanation: catalyst considerations." Catalysis today 215 (2013): 233-238.
[22] Sun, Duo, Faisal Mohamed Khan, and David S. A. Simakov. "Heat removal and catalyst deactivation in a Sabatier reactor for chemical fixation of CO_2: Simulation-based analysis." Chemical Engineering Journal 329 (2017): 165-177.
[23] Willumsen, Hans C. "Energy recovery from landfill gas in Denmark and worldwide." LG Consultant (2001).
[24] Speight, James G., ed. The biofuels handbook. Royal Society of Chemistry, 2011: 456-457.
[25] Al Seadi, Teodorita, et al. Biogas Handbook. University of Southern Denmark Esbjerg. ISBN 978-87-992962-0-0, 2008.
[26] Sun, Qie, et al. "Selection of appropriate biogas upgrading technology-a review of biogas cleaning, upgrading and utilisation." Renewable and Sustainable Energy Reviews 51 (2015): 521-532.
[27] Chen, Xiaodong, et al. "Catalytic performance of the Pt/TiO_2 catalysts in reverse water gas shift reaction: Controlled product selectivity and a mechanism study." Catalysis Today 281 (2017): 312-318.
[28] Goguet, Alexandre, et al. "Study of the origin of the deactivation of a Pt/CeO_2 catalyst during reverse water gas shift (RWGS) reaction." Journal of Catalysis 226.2 (2004): 382-392.
[29] Barreiro, M. M., M. Maroño, and J. M. Sánchez. "Hydrogen permeation through a Pd-based membrane and RWGS conversion in H_2/CO_2, $H_2/N_2/CO_2$ and $H_2/H_2O/CO_2$ mixtures." International Journal of Hydrogen Energy 39.9 (2014): 4710-4716.
[30] M. Saito, "R&D activities in Japan on methanol synthesis from CO_2 and H_2." Catalysis Surveys from Japan 2 (1998) 175-184.
[31] M.V. Twigg, M.S. Spencer, "Deactivation of copper metal catalysts for methanol decomposition, methanol steam reforming and methanol synthesis." Topics in Catalysis 22 (2003) 191-203.
[32] C. Bartholomew, Catalyst deactivation and regeneration, Kirk-Othmer Encyclopedia of Chemical Technology, 2003, pp. 13-15.
[33] M. Saito, K. Murata, "Development of high performance Cu/ZnO-based catalysts for methanol synthesis and the water-gas shift reaction." Catalysis Surveys from Asia 8 (2004) 285-294.
[34] F.S. Stone, D. Waller, "Cu–ZnO and $Cu–ZnO/Al_2O_3$ catalysts for the reverse water-gas shift reaction. The effect of the Cu/Zn ratio on precursor characteristics and on the activity of the derived catalysts." Topics in Catalysis 22 (2003) 305-318.
[35] M.J.L. Ginés, A.J. Marchi, C.R. Apesteguia, "Kinetic study of the reverse water-gas shift reaction over $CuO/ZnO/Al_2O_3$ catalysts." Applied Catalysis A: General 154 (1997) 155-171.
[36] C.-S. Chen, W.-H. Cheng, S.-S. Lin, "Mechanism of CO formation in reverse water–gas shift reaction over Cu/Al_2O_3 catalyst." Catalysis Letters 68 (2000) 45-48.
[37] Bligaard, T., et al. "The Brønsted–Evans–Polanyi relation and the volcano curve in heterogeneous catalysis." Journal of Catalysis 224.1 (2004): 206-217.
[38] Mills, G. Alex, and Fred W. Steffgen. "Catalytic methanation." Catalysis Reviews 8.1 (1974): 159-210.

[39] Garbarino, Gabriella, et al. "Methanation of carbon dioxide on Ru/Al_2O_3 and Ni/Al_2O_3 catalysts at atmospheric pressure: Catalysts activation, behaviour and stability." International Journal of Hydrogen Energy 40.30 (2015): 9171-9182.
[40] Amin, Mohamad Hassan, et al. "Highly stable ytterbium promoted $Ni/\gamma\text{-}Al_2O_3$ catalysts for carbon dioxide reforming of methane." Applied Catalysis B: Environmental 119 (2012): 217-226.
[41] Muroyama, Hiroki, et al. "Carbon dioxide methanation over Ni catalysts supported on various metal oxides." Journal of Catalysis 343 (2016): 178-184.
[42] Weatherbee, Gordon D., and Calvin H. Bartholomew. "Hydrogenation of CO_2 on group VIII metals: IV. Specific activities and selectivities of silica-supported Co, Fe, and Ru." Journal of Catalysis 87.2 (1984): 352-362.
[43] Takezawa, Nobutsune, et al. "Methanation of carbon dioxide: Preparation of Ni/MgO catalysts and their performance." Applied catalysis 23.2 (1986): 291-298.
[44] Son, In Hyuk, et al. "Study on coke formation over $Ni/\gamma\text{-}Al_2O_3$, $Co\text{-}Ni/\gamma\text{-}Al_2O_3$, and $Mg\text{-}Co\text{-}Ni/\gamma\text{-}Al_2O_3$ catalysts for carbon dioxide reforming of methane." Fuel 136 (2014): 194-200.
[45] Oshikawa, Katsuhiko, Masatoshi Nagai, and Shinzo Omi. "Characterization of molybdenum carbides for methane reforming by TPR, XRD, and XPS." The Journal of Physical Chemistry B 105.38 (2001): 9124-9131.
[46] Xiang, Minglin, and Juan Zou. "CO hydrogenation over transition metals (Fe, Co, or Ni) modified K/Mo_2C catalysts." Journal of Catalysts 2013 (2013).
[47] Xu, Wenqian, et al. "The carburization of transition metal molybdates ($MxMoO_4$, M= Cu, Ni or Co) and the generation of highly active metal/carbide catalysts for CO_2 hydrogenation." Catalysis Letters 145.7 (2015): 1365-1373.
[48] Kim, Seok Ki, et al. "Understanding the low-overpotential production of CH_4 from CO_2 on Mo_2C Catalysts." Acs Catalysis 6.3 (2016): 2003-2013.
[49] Saito, M., and R. B. Anderson. "The activity of several molybdenum compounds for the methanation of CO." Journal of Catalysis 63.2 (1980): 438-446.
[50] Vannice, M. A. "The catalytic synthesis of hydrocarbons from carbon monoxide and hydrogen." Catalysis Reviews—Science and Engineering 14.1 (1976): 153-191.
[51] Kwak, Ja Hun, Libor Kovarik, and János Szanyi. "CO_2 reduction on supported Ru/Al_2O_3 catalysts: cluster size dependence of product selectivity." ACS Catalysis 3.11 (2013): 2449-2455.
[52] Gao, Jiajian, et al. "Recent advances in methanation catalysts for the production of synthetic natural gas." RSC Advances 5.29 (2015): 22759-22776.
[53] Zhen, Wenlong, et al. "Enhancing catalytic activity and stability for CO_2 methanation on $Ni–Ru/\gamma\text{-}Al_2O_3$ via modulating impregnation sequence and controlling surface active species." RSC Advances 4.32 (2014): 16472-16479. [54]
[54] Shen, Wen-Jie, et al. "The influence of the support on the activity and selectivity of Pd in CO hydrogenation." Applied Catalysis A: General 213.2 (2001): 225-232.
[55] Vannice, M. Albert, C. C. Twu, and S. H. Moon. "SMSI effects on CO adsorption and hydrogenation on Pt catalysts: I. Infrared spectra of adsorbed CO prior to and during reaction conditions." Journal of Catalysis 79.1 (1983): 70-80.
[56] Simakov, David SA, Helen Y. Luo, and Yuriy Román-Leshkov. "Ultra-low loading $Ru/\gamma\text{-}Al_2O_3$: a highly active and stable catalyst for low temperature solar thermal reforming of methane." Applied Catalysis B: Environmental 168 (2015): 540-549.
[57] Yoshida, Hiroshi, et al. "Selective methanation of CO in H_2-rich gas stream by synthetic nickel-containing smectite based catalysts." Applied Catalysis B: Environmental 162 (2015): 93-97.

[58] P. Panagiotopoulou, D.I. Kondarides, X.E. Verykios, "Selective methanation of CO over supported Ru catalysts." Applied Catalysis B: Environmental 88 (2009) 470-478.
[59] M.B. Fichtl, D. Schlereth, N. Jacobsen, I. Kasatkin, J. Schumann, M. Behrens, R. Schlögl, O. Hinrichsen, "Kinetics of deactivation on $Cu/ZnO/Al_2O_3$ methanol synthesis catalysts." Applied Catalysis A: General 502 (2015) 262-270.
[60] M.D. Porosoff, X. Yang, J.A. Boscoboinik, J.G. Chen, "Molybdenum carbide as alternative catalysts to precious metals for highly selective reduction of CO_2 to CO." Angewandte Chemie International Edition 53 (2014) 6705-6709.
[61] Demirbas, Ayhan. Methane gas hydrate: as a natural gas source. Springer London, 2010.